Space Sci Rev (2012) 170:739–773
DOI 10.1007/s11214-012-9891-3

Surface Properties of the Mars Science Laboratory Candidate Landing Sites: Characterization from Orbit and Predictions

R.L. Fergason · P.R. Christensen · M.P. Golombek · T.J. Parker

Received: 17 October 2011 / Accepted: 13 April 2012 / Published online: 26 May 2012

Abstract This work describes the interpretation of THEMIS-derived thermal inertia data at the Eberswalde, Gale, Holden, and Mawrth Vallis Mars Science Laboratory (MSL) candidate landing sites and determines how thermophysical variations correspond to morphology and, when apparent, mineralogical diversity. At Eberswalde, the proportion of likely unconsolidated material relative to exposed bedrock or highly indurated surfaces controls the thermal inertia of a given region. At Gale, the majority of the landing site region has a moderate thermal inertia (250 to 410 $\mathrm{J\,m^{-2}\,K^{-1}\,s^{-1/2}}$), which is likely an indurated surface mixed with unconsolidated materials. The primary difference between higher and moderate thermal inertia surfaces may be due to the amount of mantling material present. Within the mound of stratified material in Gale, layers are distinguished in the thermal inertia data; the MSL rover could be traversing through materials that are both thermophysically and compositionally diverse. The majority of the Holden ellipse has a thermal inertia of 340 to 475 $\mathrm{J\,m^{-2}\,K^{-1}\,s^{-1/2}}$ and consists of bed forms with some consolidated material intermixed. Mawrth Vallis has a mean thermal inertia of 310 $\mathrm{J\,m^{-2}\,K^{-1}\,s^{-1/2}}$ and a wide variety of materials is present contributing to the moderate thermal inertia surfaces, including a mixture of bedrock, indurated surfaces, bed forms, and unconsolidated fines. Phyllosilicates have been identified at all four candidate landing sites, and these clay-bearing units typically have a similar thermal inertia value (400 to 500 $\mathrm{J\,m^{-2}\,K^{-1}\,s^{-1/2}}$), suggesting physical properties that are also similar.

Keywords Mars · Surface properties · Thermal inertia · MSL

R.L. Fergason (✉)
Astrogeology Science Center, U.S. Geological Survey, 2255 N. Gemini Drive, Flagstaff, AZ 86001, USA
e-mail: rfergason@usgs.gov

P.R. Christensen
Mars Space Flight Facility, Arizona State University, PO Box 876305, Tempe, AZ 86287-6305, USA

M.P. Golombek · T.J. Parker
Jet Propulsion Laboratory, California Institute of Technology, 4800 Oak Grove Drive, Pasadena, CA 91109, USA

1 Introduction

The main science objective of the Mars Science Laboratory (MSL) is to explore and quantitatively assess the habitability and environmental history of a local region on the martian surface. This mission will use a variety of instruments carried on a rover platform that are designed to assess the biological potential, characterize the geology, investigate planetary processes that influence habitability, and characterize the broad spectrum of surface radiation at the landing site. An ideal MSL landing site would (1) contain evidence suggestive of a past or present habitable environment; (2) meet or exceed all engineering and safety constraints; and (3) allow acceptable operational performance. In addition, it is ideal that the evidence for habitability, whether geological, chemical, or biological, would be preserved for, accessible to, and measurable and/or observable by the MSL payload. The MSL was launched on 26 November 2011 (GMT), and will arrive at Mars on 6 August 2012 (GMT). The primary science mission is one Mars year (669 Mars sols or 687 Earth days) (Grotzinger et al. 2012).

The selection of the MSL landing site began in June 2006, when the public was solicited to suggest locations on Mars for consideration. Over 60 sites were proposed, and over the course of 5 landing site workshops attended by members of the Mars science and engineering community (June 2006, October 2007, September 2008, September 2010, and May 2011) the list was narrowed to four candidate sites (see Grant et al. 2011 and Golombek et al. 2012 for additional detail). These four sites, Eberswalde, Gale, Holden, and Mawrth Vallis, are discussed in this paper. We are discussing the final four sites, rather than Gale only, because this work contributed to the process by which the final site was selected (Golombek et al. 2012) and it is important to report these finding in that context. In addition, each of these four sites remains an interesting scientific target for future exploration and it is therefore worthwhile to share these results with the planetary community. In parallel with these workshops, the scientific and engineering community investigated the candidate landing sites through the California Institute of Technology's Jet Propulsion Laboratory's Critical Data Products program. The Critical Data Product investigators generated and interpreted data sets considered critical for certifying that a location is safe for landing, trafficable by the MSL rover, and appropriate for the MSL science payload. The results of these investigations were typically presented at the workshops, and helped to inform the discussion and refinement of the landing site selection. In July 2011, NASA announced that the MSL rover, Curiosity, will land at Gale crater. Therefore, more emphasis is placed on the results and discussion of Gale than the remaining three candidate landing sites.

The goal of this work was to improve the understanding of the physical characteristics of the surface at the candidate landing sites and assess their scientific potential and engineering safety. This objective was addressed by: (1) creating a qualitative (8-bit) and quantitative (32-bit) Thermal Emission Imaging System (THEMIS)-derived thermal inertia map for each candidate site; (2) creating THEMIS-derived predicted brightness temperature images to model surface temperatures for a selected range of seasons and local times to model the minimum and maximum surface temperatures expected at each candidate site; and (3) identifying and assessing surface materials using thermal inertia, predicted temperature maps, and visible images. Thermal inertia and predicted temperature are not standard data products produced by the Mars Odyssey mission, yet these data sets have played an important role in the selection of the Mars Exploration Rover (MER), and Mars Science Laboratory (MSL) landing sites (e.g. Golombek et al. 2003, 2005). THEMIS-derived thermal inertia values were used to interpret the surface characteristics of the sites and identify potential hazards for lander safety and traversability. Examples include the presence of very dusty (or

dust dominated) surfaces (thermal inertia <100 J m^{-2} K^{-1} s$^{-1/2}$ and dust thickness greater than a few mm), which may not be load bearing or trafficable by a rover, and the presence of hazards, such as rocky and dusty materials. In addition, features, particularly layered materials observed in high-resolution visible images and regions where phyllosilicate-bearing surfaces have been identified, were assessed for their scientific importance.

In this manuscript, the results are described in terms of the physical properties of the surfaces and the impact these surfaces have on potential MSL science investigations, engineering constraints, and rover traversability. We first describe the data sets incorporated in this study and discuss the techniques used to generate THEMIS-derived thermal inertia. We then discuss each landing site individually. For each of the four final candidate landing sites, we provide a brief background and discuss the results of our analysis. We frame the discussion of our results in terms of the surface characteristics and distribution of low, moderate, and high thermal inertia regions relative to each site. To capture the widest range of surface materials at each site, the displayed ranges of low, moderate, and high thermal inertia values are specific to each site and therefore differ between sites. We then summarize our findings.

2 Data Sets and Method

2.1 THEMIS-Derived Thermal Inertia

The THEMIS dataset provides the highest spatial resolution thermophysical data available (100 m/pixel) and can be used to derive the thermal inertia of the surface materials and assess their physical characteristics. Thermal inertia is defined as $I = (k\rho c)^{1/2}$, where k is the thermal conductivity, ρ is the bulk density of the surface material, and c is the specific heat, and represents the resistance to change in temperature of the upper few centimeters of the surface throughout the day. Under martian atmospheric conditions, the density and specific heat of geologic materials vary by a factor of $\sim$3, whereas the conductivity varies by 3–4 orders of magnitude and therefore has the strongest influence on the thermal inertia (e.g., Wechsler and Glaser 1965; Neugebauer et al. 1971; Presley and Christensen 1997). Laboratory-derived relationships between particle size and conductivity (and thus thermal inertia) have been established (e.g., Woodside and Messmer 1961; Wechsler and Glaser 1965; Fountain and West 1970; Presley and Christensen 1997) and are used to infer an effective particle size of the surface from thermal inertia values. Fine particles have a lower thermal inertia, whereas higher thermal inertia surfaces are composed of sand, crusts, rock fragments, ice, bedrock, or a combination of these materials. Several factors can complicate the modeling of thermal inertia and make interpreting thermal inertia results challenging. These include, but are not limited to, the mixing of different particle sizes, the presence of crusts, subsurface layering and sub-pixel-scale slopes. The interpretation of thermal inertia as an effective particle size is less ambiguous if the thermal inertia is low (dust) or very high (bedrock), but many equally plausible scenarios can result in a particle size described by the moderate thermal inertia of a surface. In these instances, utilizing additional datasets such as high-resolution visible images can help constrain the interpretation of thermal inertia data. In this study, thermal inertia is particularly useful for obtaining a quantitative measure of surface properties throughout each landing ellipse and for providing insight into the materials present. Through this assessment, we are able to identify with confidence exposures of bedrock, the amount of surface dust present, and potential obstacles for rover trafficability at 100-m scales.

There are seasonal differences in thermal inertia values at all the candidate landing sites, likely due to atmospheric effects not being accounted for properly in the thermal models,

and secondarily to inhomogeneities on the surface and at depth (e.g., Putzig and Mellon 2007a, 2007b). When a mixture of materials is present at the surface (e.g., varying particle sizes or degrees of induration), each different material will conduct heat energy into and out of the subsurface at a different rate. These different conduction rates result in a different contribution of surface temperature, which will vary seasonally with the thermal flux. A detailed assessment of the contribution of these two effects on seasonal differences between THEMIS images is beyond the scope of this work. In most cases, based on the lowest thermal inertia values identified within the ellipse, thermal inertia values do not vary seasonally by more than $\sim$50 J m^{-2} K^{-1} s$^{-1/2}$. Despite these seasonal effects, the relative difference between surfaces within a single image is uncertain by only $\sim$10 J m^{-2} K^{-1} s$^{-1/2}$ (see Appendix and Fergason et al. 2006a for a more detailed description of all uncertainties). To minimize seasonal uncertainties and enable a more straightforward analysis of the surface properties at these sites, the analysis was focused on images acquired during similar seasons appropriate for each local site.

In this work, images were selected based on coverage of the ellipse and surrounding regions of interest, and images were included that are of high quality (based on visual inspection) and low instrument noise (Table 1). Nighttime temperatures only were used because the effects of albedo and sun-heated slopes have mostly dissipated throughout the night, and the thermal contrast due to differences in particle sizes are at a maximum (e.g., Kieffer et al. 1973, 1977; Jakosky 1979; Palluconi and Kieffer 1981). Standard THEMIS data processing, consisting of decompression, radiometric calibration, and systematic noise removal was applied to each image (Christensen et al. 2004). Each image was also corrected for the drift and wobble of the spacecraft (Bandfield et al. 2004; Fergason et al. 2006a). The method of Fergason et al. (2006a) was used to derive thermal inertia values from THEMIS nighttime infrared data. For additional detail, see Appendix. The analysis and interpretation of thermal inertia values was confined to the landing ellipse and surrounding regions of interest. Using ArcGIS 9.3, statistical information (minimum, maximum, mean, and standard deviation) was derived for each ellipse and surrounding areas of interest to understand the range of thermal inertia values present. Dusty and other low thermal inertia areas that might pose trafficability hazards to the rover were identified. The degree of thermophysical variation, the surface materials present, and the locations of exposed bedrock were also investigated for each landing site region.

2.2 Thermal Inertia Unit Maps

For the purposes of making equitable comparisons between the four candidate landing sites from a landability/mobility perspective, thermal inertia unit maps were generated. Using ArcGIS 9.3, THEMIS thermal inertia images were first georeferenced to a Mars Orbiter Laser Altimeter (MOLA; 128 pixels/degree) base map for each site, with a precision of plus or minus one pixel. This georeferencing allowed us to accurately correlate the thermal inertia pixels with surface features identified at the Context Camera (CTX, $\sim$6 m/pixel; Malin et al. 2007) and High Resolution Imaging Science Experiment (HiRISE, 25–60 cm/pixel; McEwen et al. 2007) image scales (e.g., dunes, exposed bedrock, indurated materials, or unconsolidated fines). From this correlation, the relative physical properties of surficial geologic materials representative of each landing ellipse were determined. THEMIS thermal inertia values were binned into four units for each site, based initially on established breaks in thermophysical properties (Mellon et al. 2000). The break points were further refined such that they correlated with four distinct surface units, as identified in visible images, while still enabling reasonable comparisons to be made of these materials between the four

Table 1 THEMIS IR images used in thermal inertia analysis and mosaic generation

Eberswalde	Gale	Holden	Mawrth Vallis
I03216002	I00988002	I02467002	I01580006
I03503019	I01325006	I03216002	I02229002
I04327002	I01350002	I04327002	I05250016
I04714019	I01687003	I06599007	I05300008
I05101005	I04346022	I06624005	I05325010
I06524004	I05020011	I06649009	I05687014
I06549023	I05769008	I06986009	I06386029
I06599007	I06568014	I07011004	I06723009
I07348006	I06593010	I07760011	I06748010
I08047020	I06880008	I10980002	I06798011
I08072011	I06955008	I14287006	I08246027
I08746005	I07242018	I14624013	I10430029
I11529019	I07267013	I17070026	I11391007
I14287006	I07292010	I18605020	I17506018
I14624013	I07317010	I22636006	I18729031
I16708012	I07654010	I25968010	I19016006
I17332015	I07679011	I26592022	I19328003
I17357009	I07704010	I26829012	I19690002
I18892005	I07991013	I26854014	I19952029
I19828017	I08453006	I29487002	I22710014
I25893019	I08790008	I30697003	I23047014
I25968010	I09938003	I31408007	I23072019
I26829012	I14281006	I31645006	I24919025
I27066011	I17376009	I31882009	I26666019
I27977004	I17613014	I31907010	I27240017
I28239002	I17663019	I34627006	I27265012
I30697003	I17950012	I36998004	I27290011
I31146008	I18262008		I27527015
I31383005	I18549006		I27552007
I31408007	I18574010		I28126030
I31645006	I19460021		I31320005
I31882009	I25650026		I35400005
I33666009	I27085019		I37122006
I34577002	I27110019		I38008007
I35201006	I27347016		
I36062005	I27372009		
I37260005	I27659007		
I38720005	I28233006		
	I28520022		
	I29119002		
	I29356002		
	I29930002		
	I29955002		

Table 1 (*Continued*)

Eberswalde	Gale	Holden	Mawrth Vallis
	I31140009		
	I31377003		
	I31402004		
	I32325004		
	I37254007		

sites. A relationship was found to exist between the thermal inertia and the physical properties inferred from both the ∼6 m/pixel CTX images and the 25-cm/pixel HiRISE images. The criteria used to infer the physical properties of the surface from visible images include the presence of bed forms, layered (and presumably consolidated) materials, and surfaces that appear eroded and may be bedrock; the appearance of craters, their rims, and ejecta; and the amount of bed forms and/or sand sheets present. Generally, the lowest values of thermal inertia correspond with surfaces represented by sandy or soil surfaces with little cohesion, such as eolian bed forms and expansive sand sheets. Surfaces with low to intermediate thermal inertia values exhibit recognizable eolian bed forms overlying possible cemented or indurated soil surfaces or sedimentary rock. Intermediate to high thermal inertia values correlate well with surfaces that appear to be well-indurated sedimentary materials lacking an unconsolidated eolian cover. The highest thermal inertia values correlate with coherent rock units or cemented sedimentary surface materials. For Holden and Eberswalde, where the same THEMIS IR images covered both sites, we used the same break points for these four thermal inertia categories. For Mawrth Vallis and Gale, the break points fall at lower thermal inertia values. At all four sites, the thermal inertia breakpoints were selected to match the four most prominent surface material types recognizable in the images.

2.3 Additional Data Sets and Methods

Many equally plausible scenarios, such as mixtures of different sized particles or the presence of crusts, can result in surfaces with moderate thermal inertia values, which are common at these sites. Therefore, as an additional constraint high-resolution visible images, including THEMIS visible (18 m/pixel; Christensen et al. 2004), narrow-angle Mars Orbiter Camera (MOC, 1.5 to 12 m/pixel; Malin et al. 1992; Malin and Edgett 2001), CTX (∼6 m/pixel; Malin et al. 2007), and HiRISE (RED filter; 25–60 cm/pixel; McEwen et al. 2007), were used to more definitively interpret the surface characteristics. This combination of thermal inertia and visible image data sets formed the basis for describing the surface characteristics and predicting the surface properties at each location. Visible images were also used to identify the locations of interesting landforms that may provide compelling evidence regarding past depositional environments, such as layered materials and delta-front deposits. The thermophysical properties of these landforms were investigated in greater detail. Thermal Emission Spectrometer (TES; Christensen et al. 1992, 2001) thermal inertia, albedo, and dust-cover index (DCI; Ruff and Christensen 2002) were generally not incorporated into this study due to the small size of the proposed landing ellipses (20 by 25 km) relative to the TES pixel size (maps binned at 8–16 pixels/degree). An effective particle size (Kieffer et al. 1973) was determined using the method described by Presley and Christensen (1997) for surfaces with a thermal inertia below 350 $\mathrm{J\,m^{-2}\,K^{-1}\,s^{-1/2}}$ and when these surfaces may potentially consist of a uniform particle size based on visible image observations (such as the presence of bed forms).

Several terms are used throughout this manuscript, and it is helpful to define these conventions. Particle sizes are described in terms of the standard Wentworth (1922) sedimentology scale. The exception to this standard is our use of the word "dust," which refers to the finest-grained materials capable of long-term transport via suspension in the modern martian atmosphere. In many instances, these particles likely fell out of atmospheric suspension and were deposited on the surface (as has been observed on both the Mars Pathfinder and Mars Exploration Rover (MER) hardware; e.g., Tomasko et al. 1999; Vaughan et al. 2010), as opposed being directly related to glacial or impact processes. Martian dust particle sizes are considered to be less than 10 μm, and are often less than 2 μm (e.g., Pollack et al. 1995; Tomasko et al. 1999; Wolff and Clancy 2003; Wolff et al. 2006). The term "bedrock" is used to represent high thermal inertia surface types that are in situ bedrock or surfaces dominated by rocks $> \sim$30 cm and thus have a similar surface temperature to bedrock (Edwards et al. 2009). Typically layers, cliffs, and other erosion-resistant morphologies are observed in visible images on these bedrock surfaces. The term "indurated" is used to describe a surface where some degree of consolidation has occurred. The degree of consolidation of an indurated surface may range from a weak crust on the surface to surfaces resistant to erosion and approaches the lithification of bedrock. Although bedrock is by its nature indurated material, not all indurated material is bedrock. "Weathered bedrock" refers to bedrock surfaces that have been mechanically or chemically altered such that the thermal inertia value is lower than that expected of bedrock (Fergason et al. 2006b). The term "soil" is used here to denote the finer fraction of the martian regolith and does not imply organic content (e.g., Squyres et al. 2004; Bandfield et al. 2011).

3 Eberswalde Crater

3.1 Background

Eberswalde is a degraded crater containing evidence for an ancient drainage system likely Hesperian in age (e.g., Malin and Edgett 2003; Jerolmack et al. 2004; Lewis and Aharonson 2006; Pondrelli et al. 2008). The proposed landing ellipse is centered at 23.86° S, 326.73° E. Although fluvial deposits are accessible within the ellipse, the science in the landing ellipse is secondary to that outside of the ellipse.

To the west of the ellipse is a stratified deposit that has been interpreted as a lithified delta (e.g., Malin and Edgett 2003). This series of extensive, overlapping deposits has been interpreted as the exhumed and/or eroded remnant of a fluvial distributary delta (Malin and Edgett 2003) or an aggradational delta (Lewis and Aharonson 2006). Stratigraphic layers are present throughout the delta potentially representing a wide range of geologic ages. These layers would provide the opportunity to study a preserved record of local geologic processes and the climatic and possibly biologic history of this region. The delta appears to be an erosional remnant (Malin and Edgett 2003), implying that the original delta may have been much more extensive (Jerolmack et al. 2004). In addition, phyllosilicate minerals have been identified in bottom bed sets from each lobe of the delta (Milliken and Bish 2010). The association of fluvial morphologic features with clay mineralogy indicates the transport and accumulation of fine-grained material, which can be conducive to preserving organic material. This association suggests a greater potential for the discovery of past environments that may have been habitable for life.

3.2 Results and Discussion

The mean thermal inertia of the landing ellipse is 575 J m^{-2} K^{-1} s$^{-1/2}$ with a standard deviation of 150 J m^{-2} K^{-1} s$^{-1/2}$ (Figs. 1a, 2a, Table 2). At 100 m/pixel scales, the ellipse is primarily composed of two surface components: dark, less consolidated material (thermal inertia of ∼290 to ∼360 J m^{-2} K^{-1} s$^{-1/2}$) and bright, consolidated surfaces (thermal inertia of ∼850 to ∼1090 J m^{-2} K^{-1} s$^{-1/2}$). The proportion of dark, likely unconsolidated or slightly indurated material relative to exposed bedrock or highly indurated surfaces controls the thermal inertia of a given region. So generally speaking, lower thermal inertia surfaces

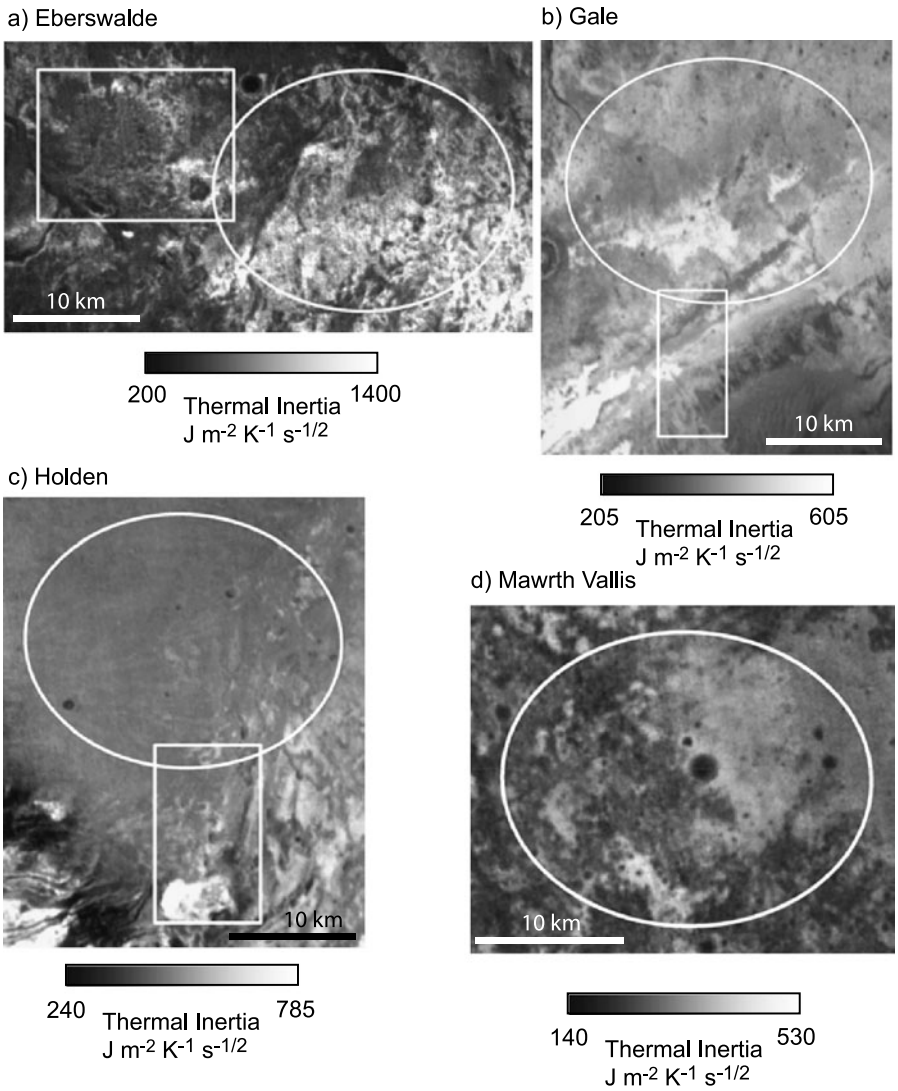

Fig. 1 Thermal inertia map of each landing site. The *white circle* indicates the location of the landing ellipse and the *white box* is the location of the primary traverse region assessed in this work. (**a**) Eberswalde; (**b**) Gale; (**c**) Holden; (**d**) Mawrth Vallis

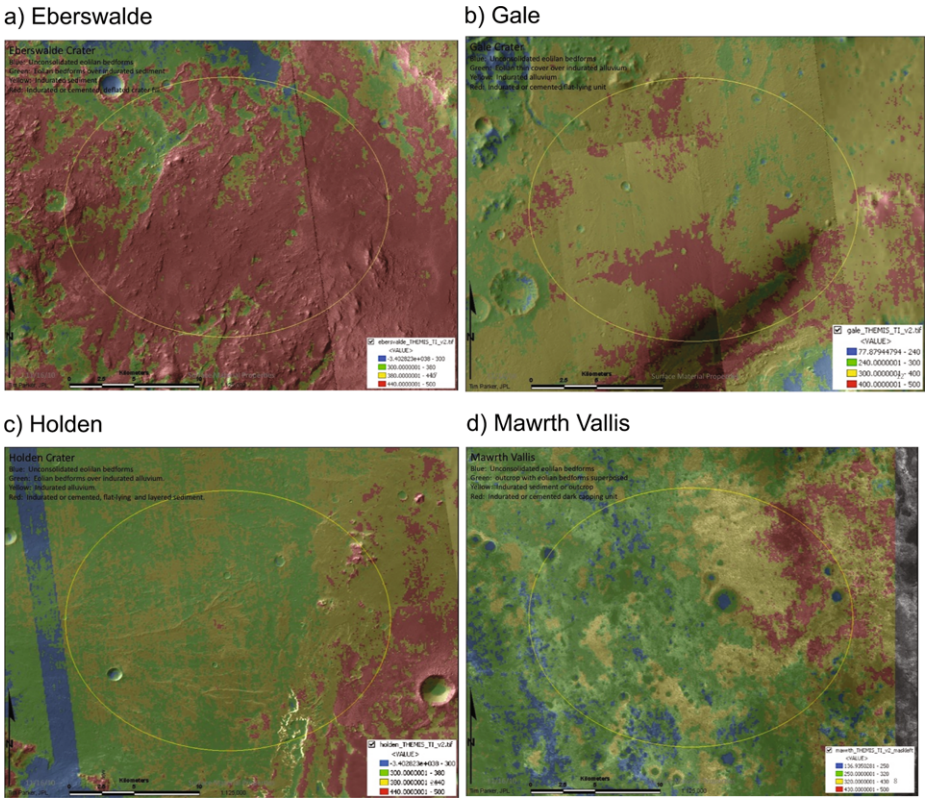

Fig. 2 Thermophyscial unit maps of each landing site. (**a**) Eberswalde; (**b**) Gale; (**c**) Holden; (**d**) Mawrth Vallis

Table 2 Summary of thermal inertia statistics

	Minimum thermal inertia ($J\,m^{-2}\,K^{-1}\,s^{-1/2}$)	Maximum thermal inertia ($J\,m^{-2}\,K^{-1}\,s^{-1/2}$)	Mean thermal inertia ($J\,m^{-2}\,K^{-1}\,s^{-1/2}$)	Thermal inertia standard deviation ($J\,m^{-2}\,K^{-1}\,s^{-1/2}$)
Eberswalde	200	1400	575	150
Gale	205	555	365	50
Holden	275	550	390	25
Mawrth Vallis	140	530	310	55

have more unconsolidated material present, typically expressed as dark deposits that usually display bed forms. Higher thermal inertia surfaces consist of more exposed bedrock or the presence of more rocky material. Moderate thermal inertia surfaces do not contain a unique surface material, and are instead similar to higher thermal inertia surfaces, only with more unconsolidated materials present, which effectively lowers the overall thermal inertia (Fig. 3).

The lowest thermal inertia value within the ellipse is 200 $J\,m^{-2}\,K^{-1}\,s^{-1/2}$, primarily found in the interior of small craters, and is interpreted as unconsolidated material. The

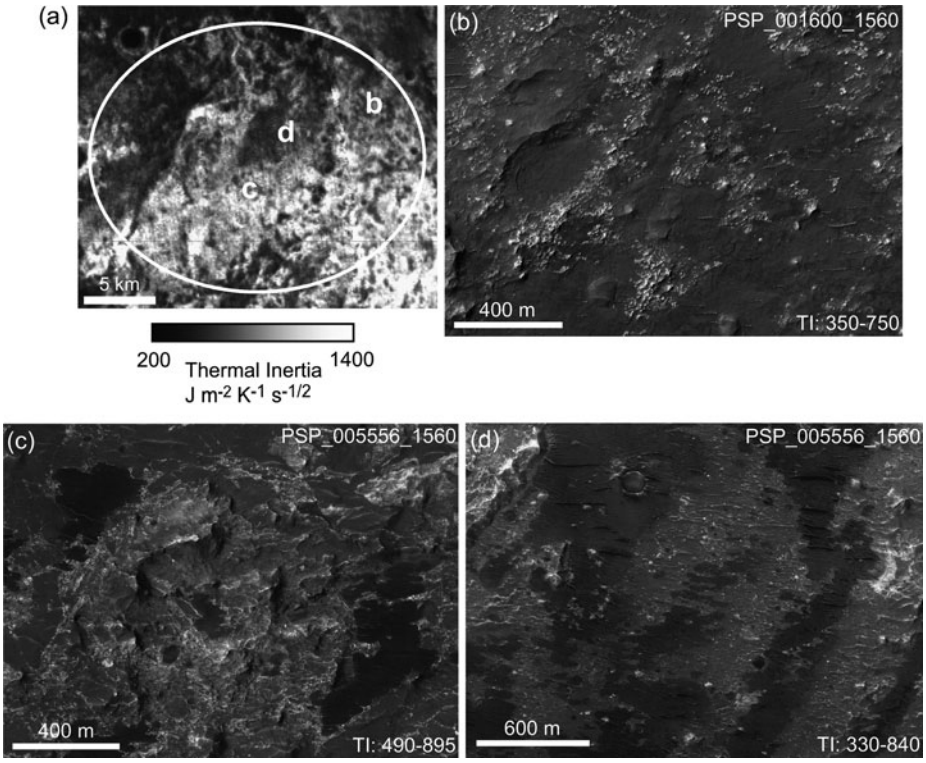

Fig. 3 Eberswalde moderate thermal inertia surfaces. These examples represent type localities of surfaces with a moderate thermal inertia. (**a**) THEMIS-derived thermal inertia mosaic of the landing site region. The *white circle* indicates the landing ellipse and *letters* indicate the location of HiRISE images (**b–d**)

presence of bed forms observed in visible data supports this interpretation. This low thermal inertia value is higher than what is expected from dust alone. Therefore, this region does not have mm-thick (or greater) dust deposits at 100-m scales. Dust could be present as a thin layer (a few micrometers in thickness), in small regions below THEMIS resolution, or be slightly indurated. The majority of lower thermal inertia surfaces range from ∼290 to ∼360 J m^{-2} K^{-1} s$^{-1/2}$ (primarily green regions in Fig. 2a) and consist of dark, smooth material that commonly displays bed forms similar to the material observed in crater interiors (Fig. 4). If this darker material is indeed unconsolidated, and assuming it consists of uniform particles, then the effective particle size is ∼780 μm (coarse sand). This material has a thermal inertia higher than expected for active dunes. The sand may either be slightly indurated or thin enough in places in so that the higher thermal inertia surface below is raising the overall thermal inertia (Fig. 4). This dark, low thermal inertia material is typically found within local depressions, such as channels and on the delta surfaces. In some places, this material is found at the base of channels originating at the crater rim. It is therefore likely that the low thermal inertia, dark, bed-forming material in the landing ellipse contains particles that originated, at least in part, from outside Eberswalde.

Thermal inertia values as high as 1400 J m^{-2} K^{-1} s$^{-1/2}$ are observed, signifying exposed bedrock present at the surface. Eberswalde is the only candidate landing site with 100-m scale bedrock exposures. This high thermal inertia material is primarily located in the southern portion of the ellipse and consists of exposed bedrock, likely indurated material, and

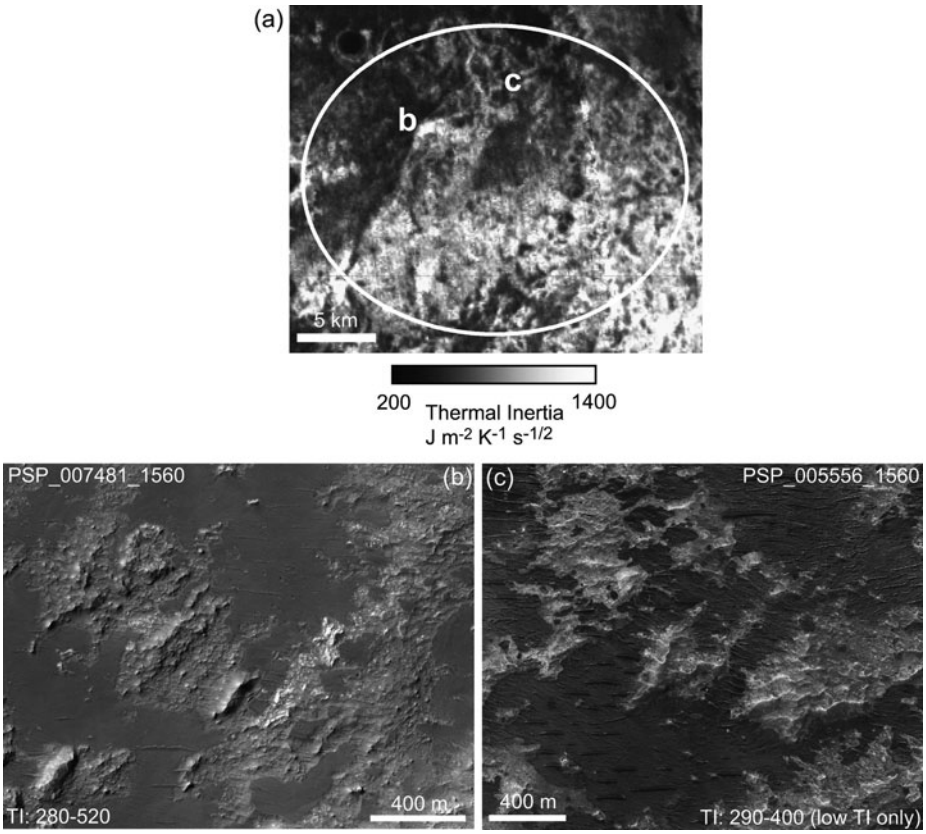

Fig. 4 Eberswalde lower thermal inertia surfaces. These examples represent type localities of surfaces with a lower thermal inertia and primarily include darker, unconsolidated material. (**a**) THEMIS-derived thermal inertia mosaic of the landing site region. The *white circle* indicates the landing ellipse and *letters* indicate the location of HiRISE images (**b–c**)

mesas/buttes with exposed layers (Fig. 5). Sand is associated with the mesas/buttes, but the bedrock surface areally dominates. In addition, less dark unconsolidated material is observed to the south, which is consistent with higher thermal inertia values in that portion of the ellipse. The dark material that is present does not typically form bed forms, and may be indurated, consist of coarser grains, or is not as thick as in the north. All of these scenarios would effectively raise the thermal inertia to values consistent with the observations.

A proposed region that the rover could investigate is the putative delta front $\sim$ 15 km west of the center of the ellipse (Fig. 6). Within the region between the ellipse and the delta, the highest thermal inertia material surrounds craters (830 to 1060 $\mathrm{J\,m^{-2}\,K^{-1}\,s^{-1/2}}$), and is present at the edge of the delta lobes (815 to 1075 $\mathrm{J\,m^{-2}\,K^{-1}\,s^{-1/2}}$). These higher thermal inertia values are associated with layered materials. The lowest thermal inertia material is confined to channels (235 to 330 $\mathrm{J\,m^{-2}\,K^{-1}\,s^{-1/2}}$), and is typically associated with pervasive bed forms. The majority of the delta itself has a moderate thermal inertia (290 to 681 $\mathrm{J\,m^{-2}\,K^{-1}\,s^{-1/2}}$), suggestive of well-indurated materials with varying amounts of unconsolidated materials intermixed.

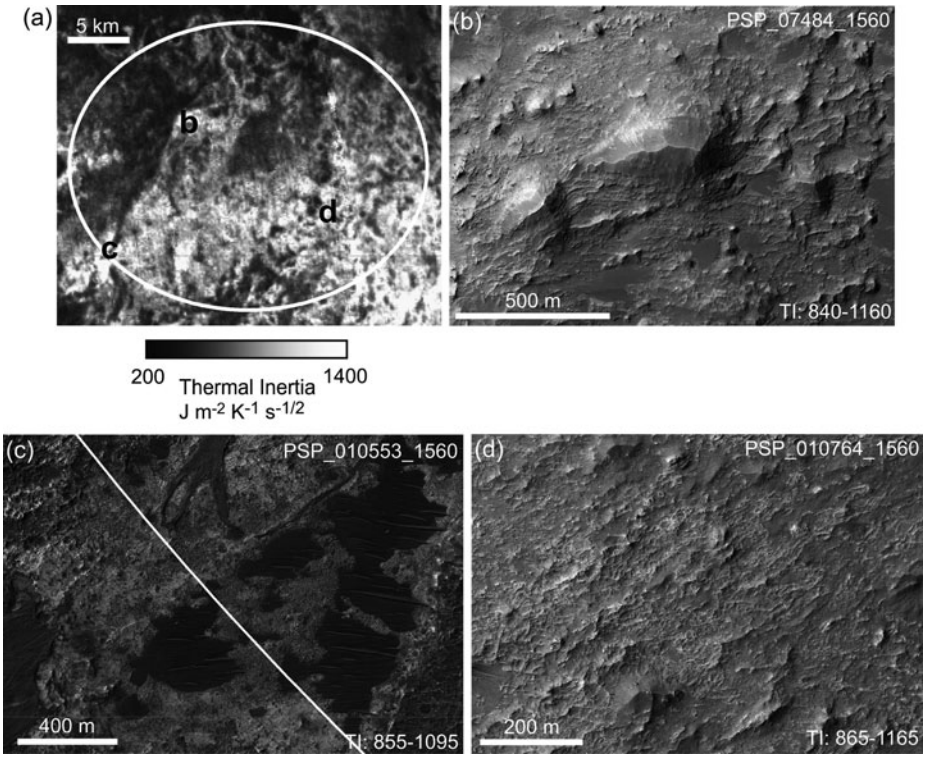

Fig. 5 Eberswalde higher thermal inertia surfaces. These examples represent type localities of surfaces with a higher thermal inertia. (**a**) THEMIS-derived thermal inertia mosaic of the landing site region. The *white circle* indicates the landing ellipse and letters indicate the location of HiRISE images (**b**–**d**). The large mounds in (*b*) are regions identified as having a high phyllosilicate spectral signature. The *white line* across image (*c*) represents the location of the landing ellipse

Two higher thermal inertia regions (Figs. 5b, 6d), one located within the ellipse and one within the delta area, are associated with clay-bearing materials (Milliken and Bish 2010; Rice et al. 2011). Within the ellipse, the clay-rich signature corresponds to exposed bedrock that has some of the highest thermal inertia values in the ellipse (thermal inertia values of 875 to 1165 J m^{-2} K^{-1} s$^{-1/2}$). This outcrop forms ridges and contains many layers and relatively bright material (as observed in visible images). Smooth material is also observed and suggests a mantle of unconsolidated or loosely consolidated material. Based on CRISM data (Milliken and Bish 2010; Rice et al. 2011), the clay-bearing material is pervasive in this region, making it difficult to determine the specific morphologic features with which the clays are associated. Thus, clays could be present as relatively bright layers, in the bedrock itself as alteration products, as a coating, or in the unconsolidated material.

Clay-bearing units identified in the delta deposits to the west of the ellipse have a thermal inertia of 545 to 730 J m^{-2} K^{-1} s$^{-1/2}$ (possibly as high as 860 J m^{-2} K^{-1} s$^{-1/2}$), and this thermal inertia range is more consistent with other clay-bearing surfaces observed at the MSL candidate landing sites. The physical properties of this clay outcrop, as viewed in HiRISE images, are significantly different than described above. Based on CRISM data, the clay signature is clearly associated with bottomset beds on the edge of the delta (Milliken and Bish 2010). The clay-bearing material is relatively bright and sometimes covered by darker, likely

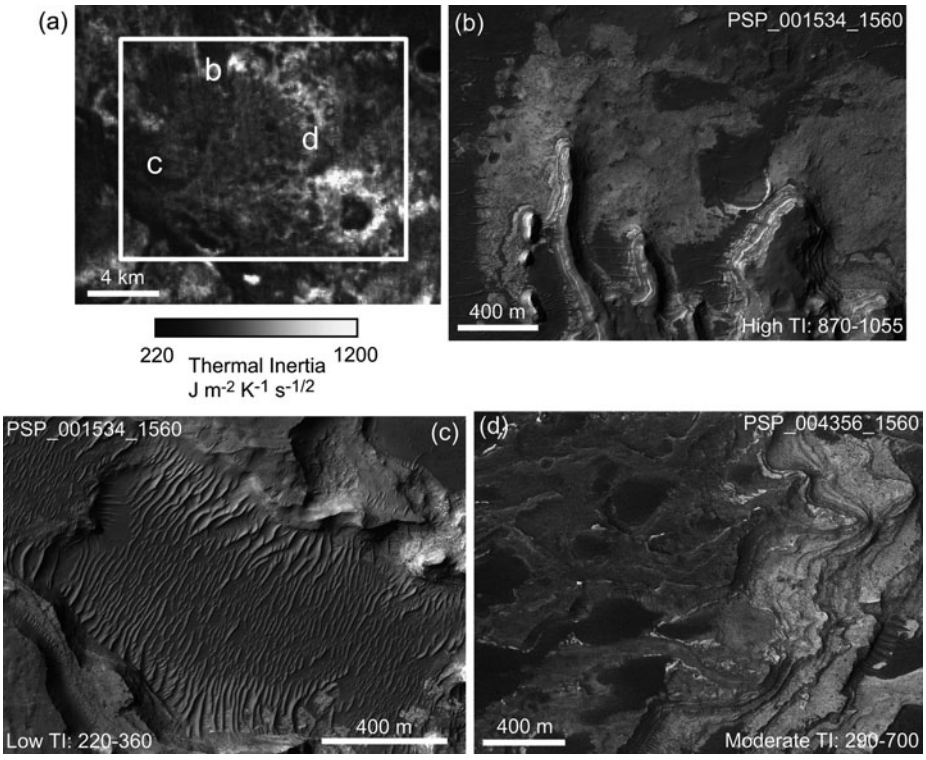

Fig. 6 Proposed Eberswalde traverse. These examples represent the range of materials observed along a proposed traverse route to the delta front region. (**a**) THEMIS-derived thermal inertia mosaic of the delta front region. The *white box* indicates the analysis area and letters indicate the location of HiRISE images (**b**–**d**). The *bright layers* in (*d*) are regions identified as having a high phyllosilicate spectral signature

unconsolidated material (Fig. 6d). The darker material is likely analogous to the dark, aeolian material found adjacent to the clay outcrops that fill more than one THEMIS pixel, and if one assumes it has the lowest thermal inertia in the region, it has a thermal inertia of 400 to 450 $\mathrm{J\,m^{-2}\,K^{-1}\,s^{-1/2}}$. This thermal inertia range is higher than expected for unconsolidated material, so either this material is indurated/cemented or, more likely, there is sub-pixel mixing at 100-m scales between the aeolian material and adjacent consolidated outcrops. Because of this sub-pixel mixing, it is challenging to determine the actual thermal inertia of these materials and get a clear picture of the physical properties of these clay-bearing surfaces. Therefore, the observed thermal inertia values of 545 to 730 $\mathrm{J\,m^{-2}\,K^{-1}\,s^{-1/2}}$ for clay-bearing units in the delta are likely an underestimation.

4 Gale Crater

4.1 Background

Gale is a Late Noachian to Late Noachian/Early Hesperian-aged crater (Thomson et al. 2011) on the dichotomy boundary between the heavily cratered southern highlands and northern lowlands, and has been selected as the landing site for MSL. A prominent mound

in its interior is ∼5 km high and is similar in height to the south rim and up to several kilometers higher than the north rim of Gale. The landing ellipse is centered at 4.5° S, 137.4° E and is located to the northwest of the mound. This mound is extensively layered and is broadly considered to be sedimentary in origin (Malin and Edgett 2000). The origin of these layers has been interpreted as aeolian (Greeley and Guest 1987; Scott and Chapman 1995), volcanic airfall ash (Scott and Chapman 1995), interbedded lava flows (Greeley and Guest 1987), lacustrine (Cabrol and Grin 1999; Cabrol et al. 1999; Malin and Edgett 2000), spring mound (Rossi et al. 2008), and ancient polar deposits (Schultz and Lutz 1988). In addition, these layers contain alternating sulfate- and phyllosilicate-bearing beds that indicate changing aqueous environmental conditions throughout Gale's history (Milliken et al. 2010). The science potential within the landing ellipse is generally considered secondary to that within the mound material.

Gale is similar to many partially filled craters on Mars and can potentially help us to better understand the family of craters with layered mounds in their interior, including Henry (e.g., Malin and Edgett 2000; Fergason and Christensen 2008), Becquerel (e.g., Malin and Edgett 2000; Lewis et al. 2008), and Terby (e.g., Malin and Edgett 2000; Wilson et al. 2007). The layers in Gale's central mound provide an opportunity to study an extensive sedimentary stratigraphic section that records the local geologic, climatic, and possibly biologic history. In addition, these layers may also record the transition from an environment favorable to clay mineral formation to one more favorable to forming sulfates and other salts (Milliken et al. 2010), which may represent global transitions in aqueous and climactic conditions on Mars (such as those described by Bibring et al. 2006).

4.2 Results and Discussion

The mean thermal inertia in the Gale landing ellipse is 365 $J\,m^{-2}\,K^{-1}\,s^{-1/2}$ with a standard deviation of 50 $J\,m^{-2}\,K^{-1}\,s^{-1/2}$ (Figs. 1b, 2b, Table 2). The majority of the ellipse has a moderate thermal inertia (250 to 410 $J\,m^{-2}\,K^{-1}\,s^{-1/2}$). The surface texture within this moderate range is consistent throughout the majority of the ellipse, and a standard deviation of 50 $J\,m^{-2}\,K^{-1}\,s^{-1/2}$ further supports the interpretation that this surface is relatively uniform. This typical, moderate thermal inertia surface appears extensively degraded in visible images and is hummocky in places, likely indurated, possibly layered, has varying amounts of dark, unconsolidated material intermixed, and in places has a smoothed appearance suggestive of a surface mantle (Fig. 7, primarily yellow regions in Fig. 2b). Outcrops of higher standing material are observed throughout the ellipse (Fig. 7b, 7d), and suggest that this area was once covered by a layer of material that was more extensive. It is therefore possible that this observed surface degradation was caused by the burial and removal of mound material that previously filled Gale.

The lower thermal inertia material represents a small fraction of the ellipse and is observed in two locations. First, low thermal inertia material is found infilling craters and depressions (205 to 250 $J\,m^{-2}\,K^{-1}\,s^{-1/2}$, corresponding to an effective particle size of 175 μm to 415 μm; fine to medium sand). This material exhibits bed forms, and is likely unconsolidated or weakly indurated (Fig. 8b; blue regions in Fig. 2b). It has a brightness similar to the surrounding region, suggestive of a thin surface mantle. Second, lower thermal inertia surfaces are associated with dark, unconsolidated material observed in the southern portion of the ellipse as a prominent NE-SW-trending deposit (250 $J\,m^{-2}\,K^{-1}\,s^{-1/2}$ to 315 $J\,m^{-2}\,K^{-1}\,s^{-1/2}$, corresponding to an effective particle size of 415 μm to 1110 μm; medium sand to very coarse sand; Fig. 8c). This value is consistent with particle sizes calculated from other studies (Hobbs et al. 2010). This thermal inertia value was determined

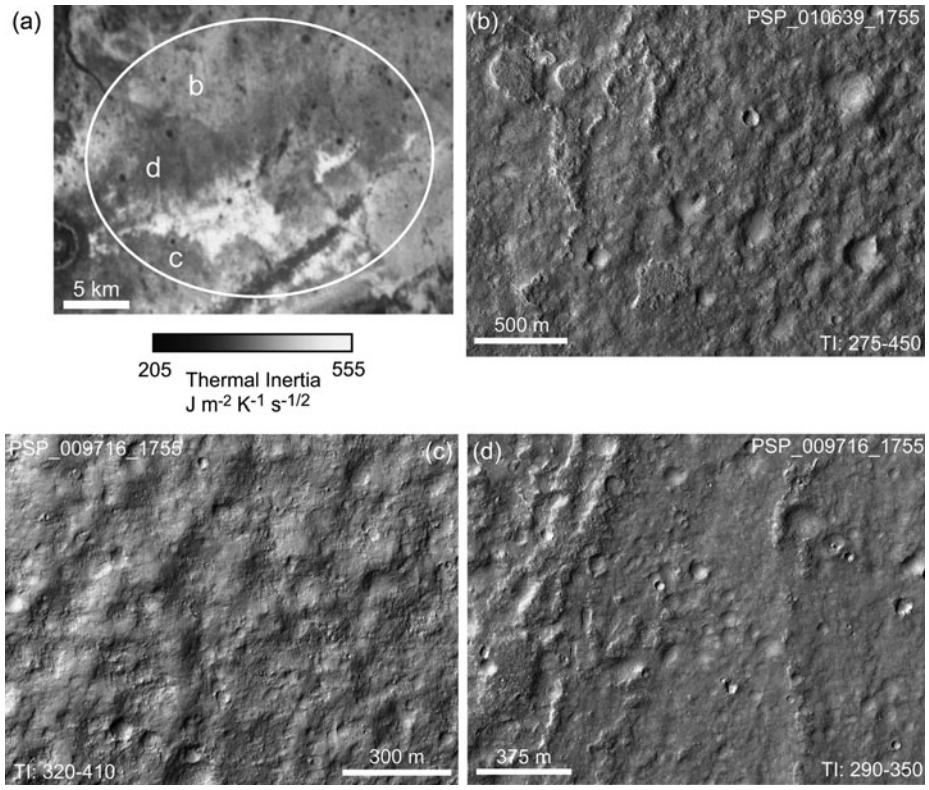

Fig. 7 Gale moderate thermal inertia surfaces. These examples represent type localities of surfaces with a moderate thermal inertia and represent the majority of surfaces within the ellipse. (**a**) THEMIS-derived thermal inertia mosaic of the landing site region. The *white circle* indicates the landing ellipse and *letters* indicate the location of HiRISE images (**b**–**d**)

from rare areas where the dark material filled the entire THEMIS field-of-view and represents the lowest thermal inertia value in the area. This value suggests that these bed-forming materials are coarser grained than expected for mobile sand (Sullivan et al. 2008). The regions sampled are typically between bed forms and may have a relatively thin sand cover where bedrock beneath the sand is raising the overall thermal inertia. It is common for the sand and exposed bedrock to both contribute to the thermal inertia at THEMIS scales. This sub-pixel mixing makes it difficult to determine an accurate thermal inertia of the dark, unconsolidated material, and is likely causing the thermal inertia value reported to result from the contribution of many sources.

The highest thermal inertia value observed in the Gale ellipse is 555 $\mathrm{J\,m^{-2}\,K^{-1}\,s^{-1/2}}$. Therefore, there are no bedrock exposures present at 100 m-scales. Bedrock exposures could be present at scales below the resolution of the THEMIS instrument. However, to remain consistent with observed thermal inertia values below 600 $\mathrm{J\,m^{-2}\,K^{-1}\,s^{-1/2}}$, those exposures must be relatively small. The higher thermal inertia surfaces ($\sim$450 to 555 $\mathrm{J\,m^{-2}\,K^{-1}\,s^{-1/2}}$) typically have a scoured appearance with little dark, unconsolidated material present (Fig. 9, red surfaces in Fig. 2b). Therefore, dark, unconsolidated material is not lowering the thermal inertia of this surface. In addition, other data sets, such as CRISM and TES DCI, are affected by a dusty component. A thin layer of dust (microns

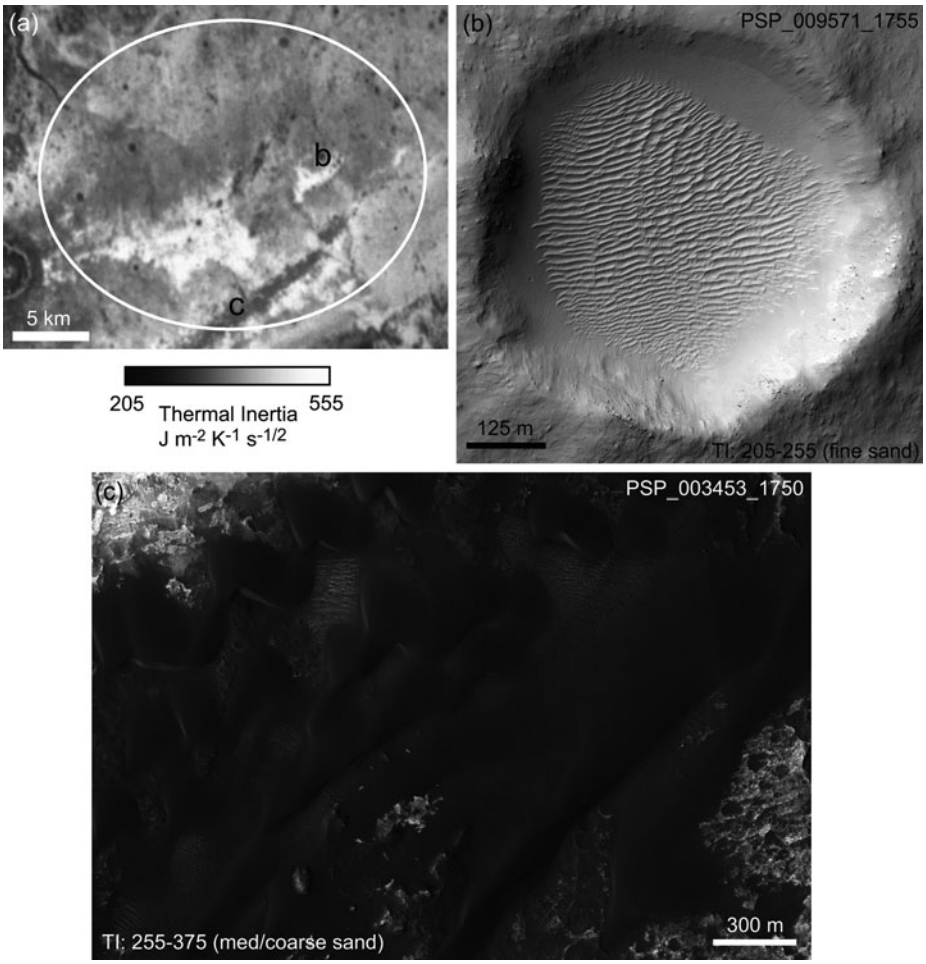

Fig. 8 Gale lower thermal inertia surfaces. These examples represent type localities of surfaces with a lower thermal inertia. (**a**) THEMIS-derived thermal inertia mosaic of the landing site region. The *white circle* indicates the landing ellipse and *letters* indicate the location of HiRISE images (**b**–**c**)

in thickness), would affect spectroscopic data from CRISM and TES, yet have a minimal effect on thermal inertia values. Since the surface brightness as observed in visible images is consistent over much of the ellipse region, this thin dust layer may be pervasive. However, the dust layer within the ellipse is likely quite thin. In addition, the thermal inertia range and degraded appearance of the surface suggest the presence of bedrock material that may be heavily weathered (Fergason et al. 2006b). The degree of induration/weathering, the amount of dark, unconsolidated material, and the variable thickness of the surface mantle are likely responsible for the range of observed thermal inertia values. This interpretation of thermophysical data sets is also consistent with previous studies using TES thermal inertia and THEMIS temperature data (Pelkey and Jakosky 2002; Pelkey et al. 2004).

Figure 9c illustrates one boundary between high and moderate thermal inertia surfaces. There is a difference in surface texture, where the moderate thermal inertia surface is

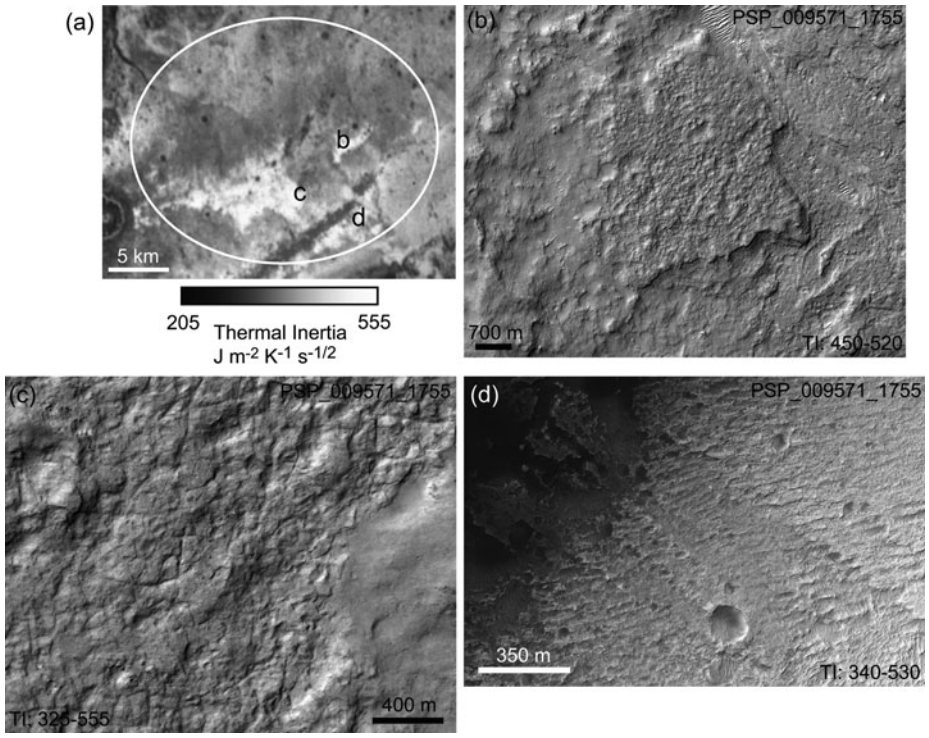

Fig. 9 Gale high thermal inertia surfaces. These examples represent type localities of surfaces with a higher thermal inertia. (**a**) THEMIS-derived thermal inertia mosaic of the landing site region. The *white circle* indicates the landing ellipse and *letters* indicate the location of HiRISE images (**b**–**d**). A typical boundary between a higher and moderate thermal inertia surfaces is illustrated in (*c*), where the smoother surface has a moderate thermal inertia and is suggestive of a surface mantle

smoother than the higher thermal inertia surface. As previously discussed, this smoothing may be caused by a mantling material that is present over much of the ellipse. To produce the degree of smoothing observed, this mantling material is likely several cm to decimeters thick, and may be moderately indurated to remain consistent with the thermal inertia values observed. It is likely that the majority of the ellipse is a complex mix of materials where the crater floor material ("bedrock") is overlain by a mantling material that may be moderately indurated, then a thin (few microns) dust layer is present as the top-most layer. This scenario would explain the observed thermal inertia values, the smooth surface, and the uniform brightness. Therefore, the primary difference between higher and moderate thermal inertia surfaces may be due to the amount of mantling material present. This relationship suggests that the mantling material likely formed in a similar way, and the post-emplacement modification of this material is the primary distinguishing factor.

In the western portion of the ellipse, an ancient fan deposit emanates from the mouth of a channel and encompasses approximately one-third of the ellipse. The fan is roughly divided in half by a lower thermal inertia (275 to 380 $\mathrm{J\,m^{-2}\,K^{-1}\,s^{-1/2}}$) portion to the north and a higher thermal inertia (395 to 555 $\mathrm{J\,m^{-2}\,K^{-1}\,s^{-1/2}}$) portion to the south. The fan boundary, as observed in HiRISE images, strongly suggests that both portions are indeed part of this ancient fan yet they have distinct thermophysical and morphological features. The entire fan is similar in brightness, suggesting a consistent albedo and possibly a very thin layer of

dust or other fine-grained mantling material. This observation is consistent with the bland spectral features observed in CRISM data (Milliken et al. 2010). The southern portion of the fan contains the largest single exposure of high thermal inertia material in the ellipse and is therefore a region of high interest to both the science and engineering communities. The higher thermal inertia material to the south contains layers, sinuous ridges, fractures (typically polygonal), boulders, appears scoured, and has little dark, aeolian material present. The lack of darker, aeolian material indicates that this fan is not currently accumulating new material from the crater walls.

The lower thermal inertia portion to the north is smoother, and may have a thicker, possibly indurated, mantle of material on its surface. This mantle is likely thin, as craters 1–2 meters in diameter are observed in HiRISE images. Generally, the smoother the surface, the lower the thermal inertia, suggesting that the mantle thickness is the primary control on thermal inertia. This observation also suggests that the higher thermal inertia surface observed to the south is present beneath the mantle to the north.

A proposed traverse ranges ∼12–20 km from the center of the ellipse towards the south and onto the lower portions of the central mound (Anderson and Bell 2010). Along the traverse up the mound individual layers are distinguished in the thermal inertia data (Fig. 10). Thus, Curiosity could be traversing through materials that are compositionally diverse with distinct surface properties associated with individual units. The mound has been previously divided into a Lower and Upper formation (Milliken et al. 2010). In this work, the Lower formation was further divided into five thermophysical units that correspond to morphological and mineralogical boundaries (Fig. 10). The lower most unit (TU1) is actually on the crater floor, contains the full range of thermal inertia values observed (265 to 490 $\mathrm{J\,m^{-2}\,K^{-1}\,s^{-1/2}}$), and corresponds to the presence of Fe-oxide. This Fe-oxide is only one component of the surface and its distribution is patchy, as observed in CRISM data (Milliken et al. 2010). The lower thermal inertia values correspond to the previously discussed dark materials in which bed forms are observed. These dark material bed forms occur both as a NE-SW trending deposit at the southern margin of the ellipse (represented by this unit) and within canyons and topographic depressions throughout the Lower formation of the mound. The higher thermal inertia values correspond to surfaces that have ridges, minimal dark material, and a scoured appearance. These observations suggest resistant, well-consolidated surfaces that should pose little difficulty in traversing.

The next unit (TU2) has a thermal inertia ranging from 330 to 420 $\mathrm{J\,m^{-2}\,K^{-1}\,s^{-1/2}}$. Both the thermal inertia values and the morphology suggest a mixture of materials including unconsolidated materials, boulders, and indurated/cemented surfaces. Some exposed bedrock may also be present, but these exposures must be small to be consistent with the thermal inertia values observed. The composition of these materials remains poorly constrained (Milliken et al. 2010). The next unit (TU3) has a slightly higher thermal inertia ranging from 355 to 485 $\mathrm{J\,m^{-2}\,K^{-1}\,s^{-1/2}}$ and corresponds to Fe-rich clays (Milliken et al. 2010). Units TU2 and TU3 are similar in morphology. The primary difference is likely the amount of unconsolidated material present, which results in slightly different thermal inertia ranges.

The next unit (TU4) is not a continuous layer, but is instead roughly circular and has the highest thermal inertia value in this region (520 to 605 $\mathrm{J\,m^{-2}\,K^{-1}\,s^{-1/2}}$). This material is topographically higher than the surrounding surface and has little to no dark, presumably unconsolidated material present. The surface texture consists of layers and ridges and has a rippled appearance, which suggests the presence of ancient bed forms (Anderson and Bell 2010). Anderson and Bell (2010) suggest that this circular outcrop is a portion of a more-extensive unit that skirts the mound. The composition is fairly unconstrained, although there is a weak pyroxene signature in CRISM data (Milliken et al. 2010). We are interpreting

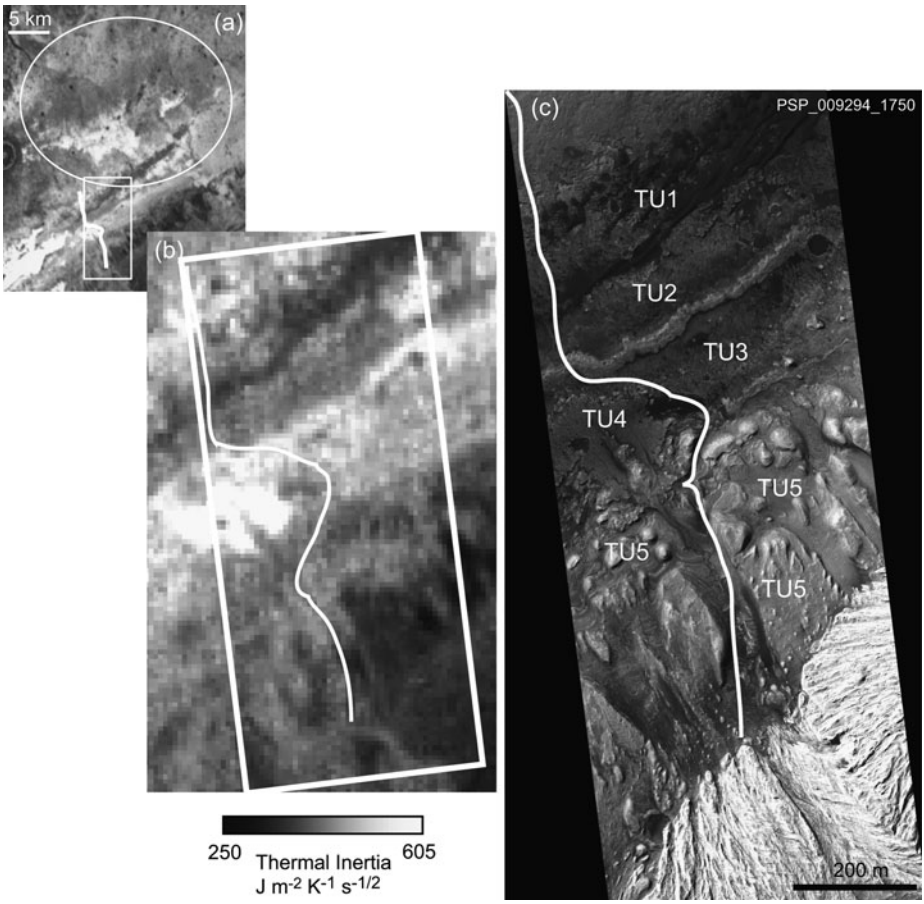

Fig. 10 Proposed Gale traverse. (**a**) THEMIS-derived thermal inertia mosaic of the landing site ellipse and potential traverse to provide context for figures (*b*) and (*c*). (**b**) THEMIS-derived thermal inertia mosaic of the region immediately surrounding (*c*) to illustrate the thermophysical diversity observed within the mound material and along a potential traverse. The *white box* indicates the approximate outline of the HiRISE image in (*c*). (**c**) HiRISE image illustrating the morphological diversity that corresponds to the thermophysical variation in (*b*). The *white line* in image (*a–c*) indicates a potential traverse route

this surface to be well indurated, representing an ancient surface that was once buried and has been exposed. In this region, slopes commonly exceed 30° further indicating that this surface is well-indurated (Golombek et al. 2012).

The last unit in the Lower formation (TU5) has a thermal inertia of 260 to 420 $\mathrm{J\,m^{-2}\,K^{-1}\,s^{-1/2}}$. This unit is extensively layered and these layers are laterally continuous and are commonly exposed in channels (which typically have dark, unconsolidated material present; TU1) and mesas. This spectrally dominant phase in this unit is sulfate (Milliken et al. 2010). The combination of extensive layers and complex compositional relationships indicates that these layers record a complex geologic history that is difficult to unravel solely from orbital data. In summary, the Lower formation of the mound contains an abundant variety of materials from a thermophysical, morphological, and compositional

perspective, and further investigation by Curiosity will help to better understand the geologic and climate history in this region.

In the mound, the Upper formation is separated from the Lower formation by an unconformity (Milliken et al. 2010) and has a thermal inertia of 120 to 260 J m^{-2} K^{-1} s$^{-1/2}$, which suggests the presence of fine-grained, loosely consolidated material and a significant portion of dust mantling the mound. In addition, this region lacks absorptions indicative of hydrated minerals and its composition is similar to that of typical martian dust (Milliken et al. 2010), which further supports this interpretation. However, thermophysical variations in the Upper formation correspond to specific layers and terraces observed in the mound. These variations may be caused by differing amounts of dark, unconsolidated material and dust present, which may be controlled by topography. The Upper formation has likely been formed by non-aqueous processes (Milliken et al. 2010). This unit typically erodes into yardangs, and similar morphologies elsewhere on Mars have been interpreted to be indurated dust (e.g., Fergason and Christensen 2008; Lewis et al. 2008). Further investigation by Curiosity may help to better understand similar intracrater deposits observed elsewhere on Mars.

5 Holden Crater

5.1 Background

Holden is a ∼140 km diameter impact crater of Noachain age (Scott and Tanaka 1986; Grant and Parker 2002) that interrupted the previously through-flowing Uzboi-Ladon-Margaritifer outflow channel system (Grant and Parker 2002). Water ponded in Uzboi Vallis by the Holden impact overflowed, breaching the crater rim (Grant and Parker 2002). The landing ellipse is centered at 26° S, 325° E, in the southeastern portion of the crater just to the north of the Uzboi Vallis breach. In addition, phyllosilicate-bearing (Milliken and Bish 2010) bright layered deposits (Grant and Parker 2002; Malin and Edgett 2000; Moore and Howard 2005) and coarse-grained alluvial fans (e.g., Grant et al. 2008; Pondrelli et al. 2005) were deposited in Holden. The clay mineral deposits are consistent with the presence of either smectite or mix-layer smectite/chlorite (Milliken and Bish 2010). These layers would provide an opportunity to study a preserved record of the regional geologic history of Margaritifer Terra, and provide insight into the climate of a wetter Mars. The continuity of the layers and their flat-lying nature further supports an origin related to deposition in standing water or a low energy fluvial environment (Grant and Parker 2002; Grant et al. 2008). An evaluation of the stratigraphy and geomorphology suggests that Holden may have contained water multiple times in its history (Pondrelli et al. 2005; Grant et al. 2008). Holden is a compelling landing site because it may preserve evidence of a closed fluvial-lacustrine system, an environment that may have been habitable (Summons et al. 2011).

5.2 Results and Discussion

The mean thermal inertia within the Holden landing ellipse is 390 J m^{-2} K^{-1} s$^{-1/2}$ with a standard deviation of 25 J m^{-2} K^{-1} s$^{-1/2}$. As indicated by the low standard deviation, the majority of the ellipse has a consistent thermal inertia and there is little variation in surface properties within the ellipse (Figs. 1c, 2c, Table 2). The vast majority of the Holden ellipse has a thermal inertia of 340 to 475 J m^{-2} K^{-1} s$^{-1/2}$ and consists of bed forms with some consolidated material intermixed (Fig. 11). The thermal inertia is greater than that expected

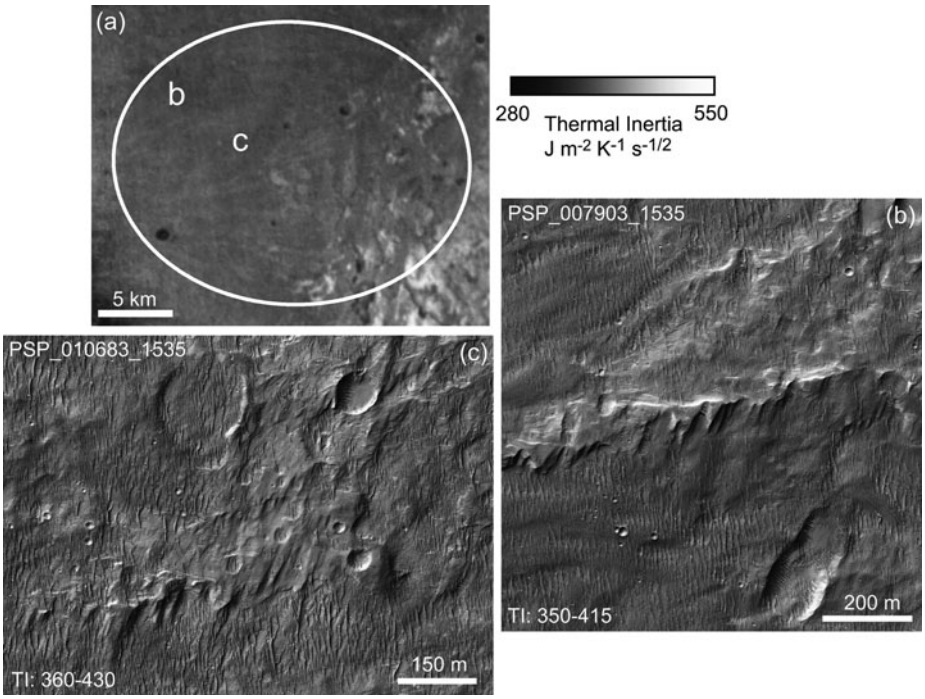

Fig. 11 Holden moderate thermal inertia surfaces. These examples represent type localities of surfaces with a moderate thermal inertia. (**a**) THEMIS-derived thermal inertia mosaic of the landing site region. The *white circle* indicates the landing ellipse and *letters* indicate the location of HiRISE images (**b**–**c**)

for eolian dunes on Mars (e.g., Edgett and Christensen 1991) and may indicate that the bed forms consist of a predominant grain size larger than sand, are indurated and no longer active, or that the thickness of the unconsolidated material is thin enough in places that the thermal inertia is influenced by underlying, well indurated material or bedrock. In addition, at THEMIS scales, the consolidated material is sometimes intermixed with the sand, thereby increasing the thermal inertia value.

The minimum thermal inertia value within the ellipse is 275 J m^{-2} K^{-1} s$^{-1/2}$, which corresponds to an effective particle size of ~620 μm or medium to coarse sand. This value is higher than what is expected for dust, and suggests that the surface is relatively dust-free. The lower thermal inertia material is limited to the interiors of some craters, where there are always bed forms present (Fig. 12, blue regions in Fig. 2c). The maximum thermal inertia value within the ellipse is 550 J m^{-2} K^{-1} s$^{-1/2}$, signifying that there are no 100-m scale bedrock exposures. These high thermal inertia instances are rare and are found primarily in the southeastern portions of the ellipse (Fig. 13; red regions in Fig. 2c). These surfaces are associated with indurated material and exposed bedrock that is extensively layered. Sub-pixel mixing between layered and unconsolidated material is lowering the overall thermal inertia from that of the layered material itself. Mechanically or chemically weathered bedrock may also be present, which could have a thermal signature lower than that of bedrock (Fergason et al. 2006b). Therefore, it is impossible to isolate the physical properties of the layered bedrock material using orbital data sets alone.

A potential traverse route exists to the south of the ellipse that includes (a) layered deposits 10 km from the center of the ellipse; (b) Uzboi flood deposits 13 km from the center of

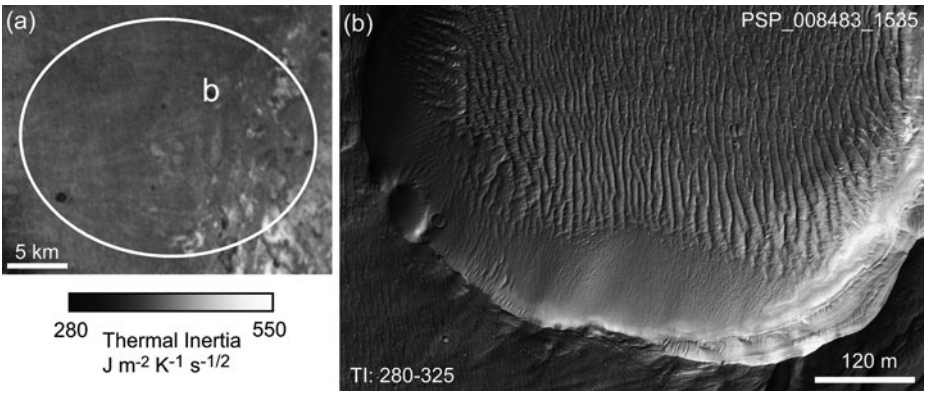

Fig. 12 Holden lower thermal inertia surfaces. This example represents a type locality of surfaces with a lower thermal inertia, which are found almost exclusively in the floors of craters. (**a**) THEMIS-derived thermal inertia mosaic of the landing site region. The *white circle* indicates the landing ellipse and the *letter* indicates the location of HiRISE image (**b**)

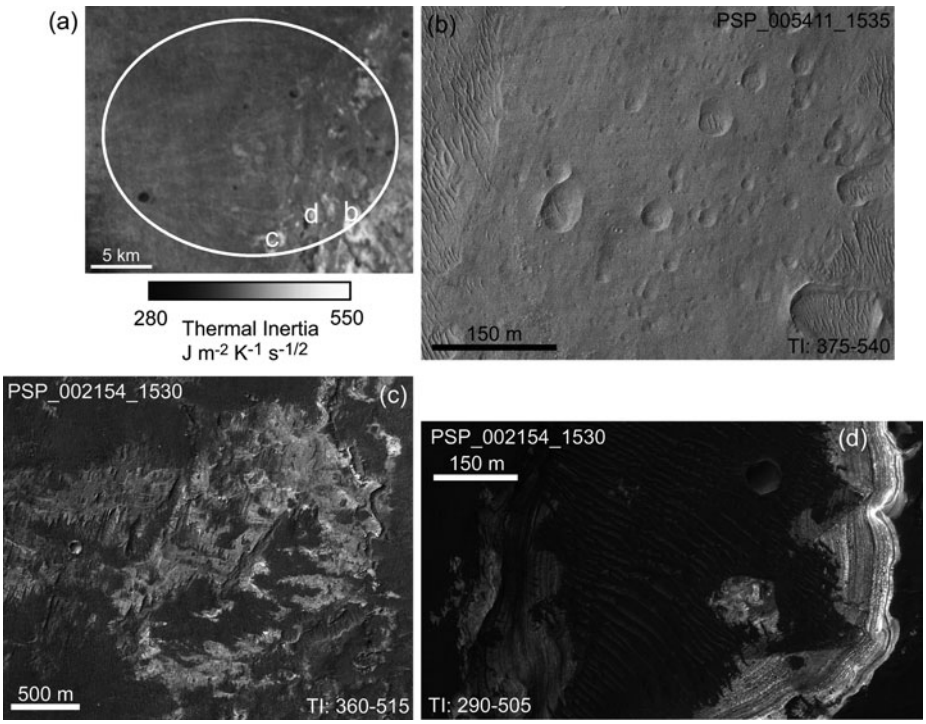

Fig. 13 Holden higher thermal inertia surfaces. These examples represent type localities of surfaces with a higher thermal inertia. (**a**) THEMIS-derived thermal inertia mosaic of the landing site region. The *white circle* indicates the landing ellipse and *letters* indicate the location of HiRISE images (**b–d**)

the ellipse; and (c) bedrock outcrops 18 km from the center of the ellipse (R. Irwin, Notional traverses and science targets in Holden crater. 3rd MSL Landing Site Workshop, Monrovia, CA, http://marsoweb.nas.nasa.gov/landingsites/msl2009/workshops/3rd_workshop/

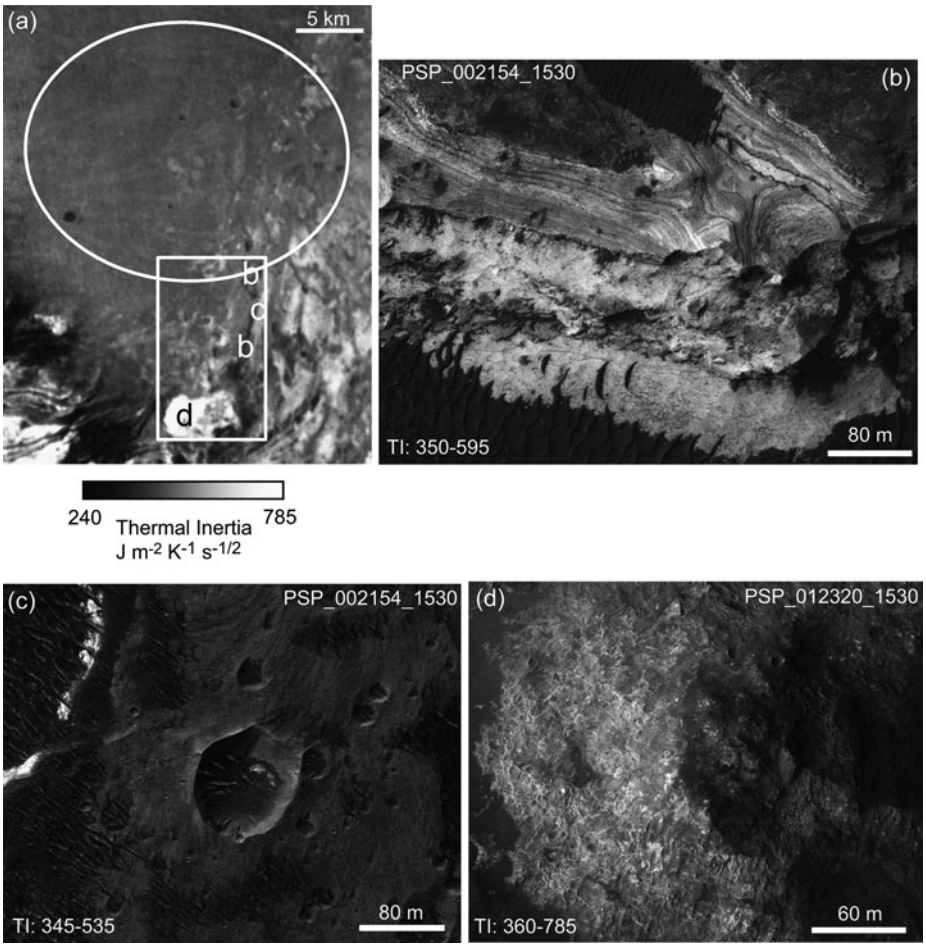

Fig. 14 Potential Holden traverse. These examples represent the range of materials observed along a proposed traverse route. (**a**) THEMIS-derived thermal inertia mosaic of the landing site and traverse region. The *white circle* indicates the landing ellipse, the white box indicates the traverse area, and letters indicate the location of HiRISE images (**b**–**d**).; (**b**) layered deposits 10 km from the center of the ellipse; (**c**) Uzboi flood deposits 13 km from the center of the ellipse; and (**d**) bedrock outcrops 18 km from the center of the ellipse

program.html (2008). Accessed 16 August 2011) (Fig. 14). Portions of the bright layered deposits have a high thermal inertia (450 to 600 J m^{-2} K^{-1} s$^{-1/2}$) and are mixed with significant amounts of sand. These deposits are similar to those found within the southern portion of the ellipse and may have been formed by the same depositional mechanism. These deposits also contain clay-bearing minerals (Milliken and Bish 2010). Due to the sub-pixel mixing of materials and the small size of the layers relative to a THEMIS footprint, it is not possible to isolate the thermal inertia of this clay-rich material with confidence. The highest thermal inertia values are ∼600 J m^{-2} K^{-1} s$^{-1/2}$, which suggests that the layers themselves are well-indurated. In addition, slopes in this region are greater than 30°, further indicating well indurated materials (Golombek et al. 2012). The layers are the brightest material in the region, are possibly fractured (with dark aeolian material filling the fractures), erode to form boulders and ridges, and appear to be relatively smooth at HiRISE scales. The layers are ap-

parent based on brightness differences. However, these differences may be due to differing amounts of dark aeolian material accumulating, rather than the properties of the indurated material itself.

The Uzboi flood deposits have thermal inertia values ranging from ∼345 to ∼480 $\mathrm{J\,m^{-2}\,K^{-1}\,s^{-1/2}}$ and are likely well indurated with some unconsolidated material present at the sub-pixel level. These materials may also be weathered, as is reflected in the moderate, rather than high, thermal inertia range. Likewise, the exposed bedrock outcrop has a thermal inertia of 530 $\mathrm{J\,m^{-2}\,K^{-1}\,s^{-1/2}}$ to 785 $\mathrm{J\,m^{-2}\,K^{-1}\,s^{-1/2}}$. Unconsolidated material is observed in visible images, lowering the observed thermal inertia values at 100-m scales. In addition, this material could be heavily weathered bedrock, but it is unlikely that weathering alone can explain the lower thermal inertia over such a large area, while remaining well preserved. Therefore a combination of weathering and the presence of unconsolidated materials is likely resulting in a lower than expected thermal inertia for this bedrock outcrop.

6 Mawrth Vallis

6.1 Background

The landing site region consists of the Mawrth Vallis channel and the surrounding ancient cratered plains dissected by the channel, and provides an opportunity to explore Noachian-age materials and probably the oldest preserved rocks at the four candidate sites. The location of the proposed landing ellipse is between a north-south segment of the channel and the crater Oyama, centered at 24° N, 341° E. A diverse set of surface materials is present within the ellipse, including bright and dark rocks and an intermediate unit. All units appear well consolidated from visible image observations (Michalski and Noe Dobrea 2007; Michalski and Fergason 2009; Michalski et al. 2010) and were likely emplaced and modified by multiple geologic processes. On the basis of infrared spectroscopy, the dark and intermediate units are composed of chemically weathered mafic materials. The intermediate surfaces are more chemically weathered than the dark unit and may also contain surface dust (Michalski and Fergason 2009).

The region in and surrounding Mawrth Vallis contains one of the largest exposures of phyllosilicates on the martian surface (Poulet et al. 2005; Bibring et al. 2006). Phyllosilicates are found within these layered, bright rocks (Poulet et al. 2005) and the environmental conditions that formed the clays may be representative of global conditions on Mars in its ancient past. Additionally, Mawrth Vallis contains Al-rich clays, which do not commonly occur on Mars (Wray et al. 2008; Milliken and Bish 2010). There are several proposed mechanisms for the origin of these layered materials, including volcanic ash fall/flow deposits, eoilian transport, fluvial transport, or impact ejecta (e.g., Michalski et al. 2010). The geology of Mawrth Vallis is complex, with little consensus regarding the depositional setting or the potential mechanism(s) for the origin of phyllosilicates. Thus, understanding the emplacement environment(s) and formation mechanism(s) for the material in this region may be an intractable problem using orbital data alone.

6.2 Results and Discussion

Within the Mawrth Vallis landing ellipse, the mean thermal inertia is 310 $\mathrm{J\,m^{-2}\,K^{-1}\,s^{-1/2}}$ with a standard deviation of 55 $\mathrm{J\,m^{-2}\,K^{-1}\,s^{-1/2}}$ (Figs. 1d, 2d, Table 2). A wide variety of materials contribute to the moderate thermal inertia surfaces, including a mixture of bedrock,

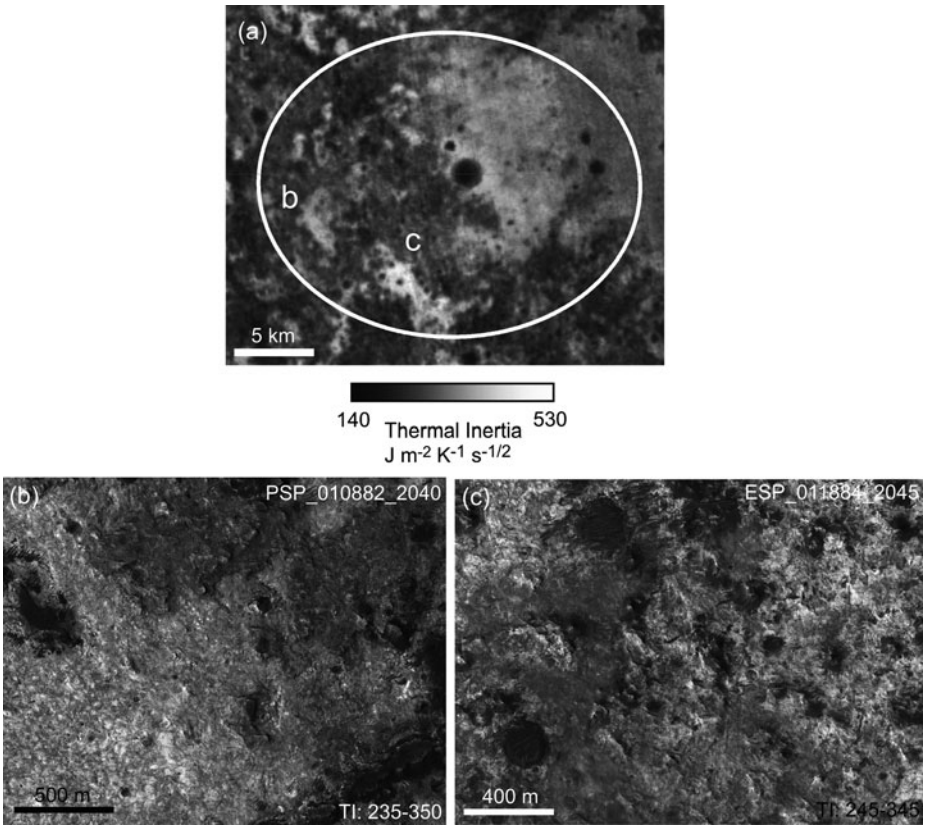

Fig. 15 Mawrth moderate thermal inertia surfaces. These examples represent type localities of surfaces with a moderate thermal inertia. (**a**) THEMIS-derived thermal inertia mosaic of the landing site region. The *white circle* indicates the landing ellipse and the *letters* indicate the location of HiRISE images (**b**–**c**)

indurated surfaces, bed forms, and unconsolidated fines (Fig. 15). It is also possible that the degree of physical weathering of bedrock varies throughout the region.

The lowest thermal inertia value is 140 J m^{-2} K^{-1} s$^{-1/2}$ and likely contains some component of dust mixed (either horizontally or vertically) with unconsolidated material. The thermal inertia value indicates that this dust layer is not thick enough to mask the contribution from underlying materials, so if present it is likely less than a few mm thick. The lower thermal inertia material is found within craters and is likely unconsolidated (Fig. 16, blue regions in Fig. 2d). The highest thermal inertia value found in the ellipse is 530 J m^{-2} K^{-1} s$^{-1/2}$ and signifies that 100 m-scale exposures of bedrock are not present at the surface. Instead, the higher thermal inertia material likely consists of smaller exposures of bedrock, indurated material, or pyroclastic deposits (Fig. 17, red regions in Fig. 2d). Minimal unconsolidated material is present on the surface in the high thermal inertia regions. So, while some bedrock is likely present, the lower thermal inertia value observed is likely due to the lower porosity of a majority of these surfaces (Fergason et al. 2006b) rather than the sub-THEMIS-pixel mixing of fine-grained material and bedrock.

Clay-bearing materials are present at this site, and this is one of the primary reasons Mawrth was considered as a potential landing site. There are two distinct clay signatures

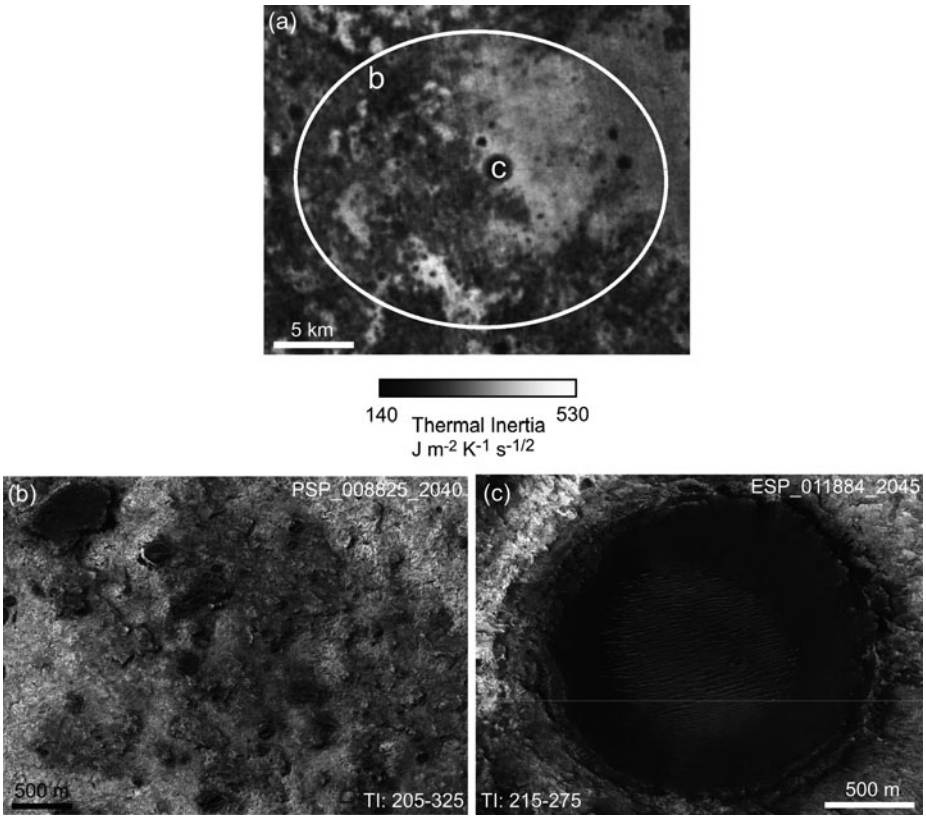

Fig. 16 Mawrth lower thermal inertia surfaces. These examples represent type localities of surfaces with a lower thermal inertia. (**a**) THEMIS-derived thermal inertia mosaic of the landing site region. The *white circle* indicates the landing ellipse and the *letters* indicate the location of HiRISE images (**b–c**)

within the landing ellipse: Fe/Mg-smectite and Al phyllosilicate (Poulet et al. 2008), and these signatures have distinct thermophysical properties. The thermal inertia of the Fe/Mg smectite-bearing material ranges from 400 to 470 $\mathrm{J\,m^{-2}\,K^{-1}\,s^{-1/2}}$ and has some of the highest thermal inertia value in the landing ellipse (approximately corresponds to yellow surfaces in Fig. 2d). There are some values as low as $\sim$370 $\mathrm{J\,m^{-2}\,K^{-1}\,s^{-1/2}}$, but these regions have dark aeolian material present that is lowering the thermal inertia as observed in THEMIS data. The Fe/Mg-smectite clays are the brightest materials in the landing ellipse and form sinuous ridges and contain fractures and polygons filled with dark, probably aeolian material. This dark material is lowering the overall thermal inertia value interpreted from THEMIS data. Therefore, the bright material is likely very well indurated. The region with Al-phyllosilicates has a variable thermal inertia ranging from 210 to 390 $\mathrm{J\,m^{-2}\,K^{-1}\,s^{-1/2}}$ (roughly corresponds to green surfaces in Fig. 2d). This material is also layered and rough, but has significantly more dark, aeolian material present on the surface. It is also not as bright as the Fe/Mg-smectite area. The variable thermal inertia and difference in brightness may both be related to the amount of unconsolidated material present and its distribution. Variable degrees of bedrock weathering may be present, affecting the thermal inertia ranges as well.

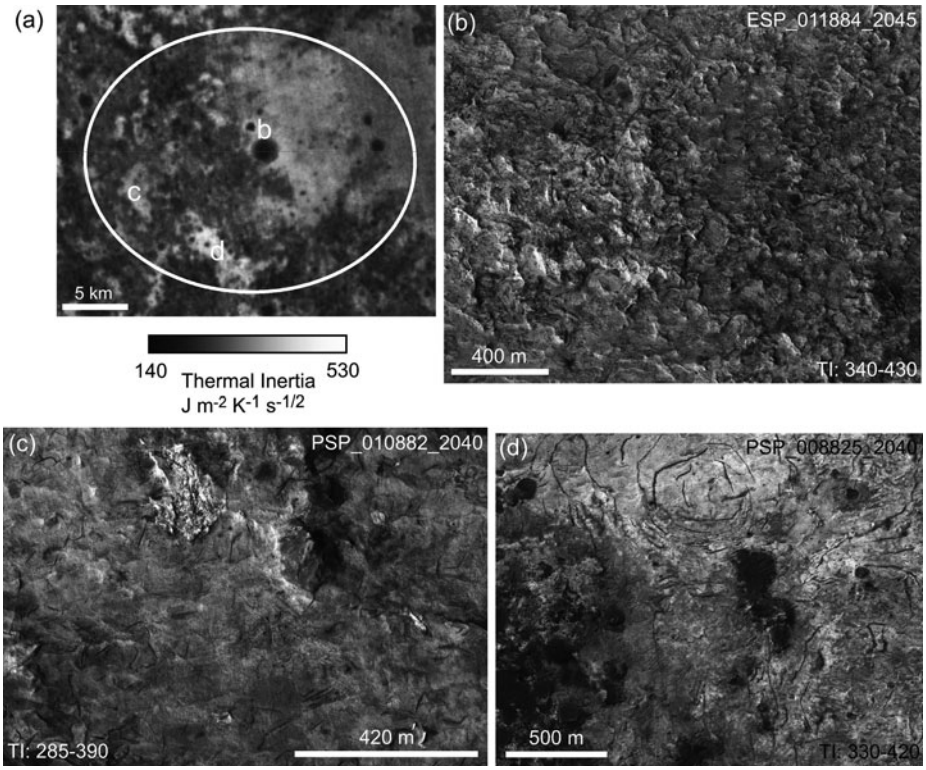

Fig. 17 Mawrth higher thermal inertia surfaces. These examples represent type localities of surfaces with a higher thermal inertia. (**a**) THEMIS-derived thermal inertia mosaic of the landing site region. The *white circle* indicates the landing ellipse and the letters indicate the location of HiRISE images (**b**–**d**)

7 Implications

7.1 Phyllosilicates at the MSL Landing Sites

Phyllosilicates are present at all four candidate landing sites (e.g., Poulet et al. 2005; Wray et al. 2008; Milliken and Bish 2010; Milliken et al. 2010), and there are several similarities across these deposits. The clay-bearing units are typically bright, layered material, and often have fractures and polygons present, thus the physical nature of these deposits are assumed to be similar. The similarities are also apparent in the thermal inertia data as all clay-bearing units have a thermal inertia value ranging from 400 to 500 $\mathrm{J\,m^{-2}\,K^{-1}\,s^{-1/2}}$, suggesting similar physical properties and surface characteristics. We interpret this moderate thermal inertia value to be consistent both with well-indurated soil or altered bedrock. In the lower Columbia Hills at the MER-A landing site, heavily altered, in-place bedrock was observed (Arvidson et al. 2006). The average thermal inertia of the in-place bedrock was $\sim$620 $\mathrm{J\,m^{-2}\,K^{-1}\,s^{-1/2}}$ (Fergason et al. 2006b), which is slightly higher than the majority of values observed at the candidate landing sites. At the landing sites, there is dark, aeolian material intermixed with most of the clay deposits at 100-m-scales. It is therefore likely that sub-pixel-mixing is lowering the apparent thermal inertia of these phyllosilicate materials and the physical characteristics may indeed be similar to deposits observed in the Columbia Hills.

There are many different formation and post-modification environments that are consistent with the inferred physical properties. These environments include, but are not limited to, bedrock that has been substantially altered by mechanical and/or chemical processes, interaction between bedrock and subsurface aquifers, ponding of water and subsequent chemical alteration of bedrock, or adsorbed water vapor forming alteration rock coatings (e.g., Gooding 1978). In addition, three out of the four candidate landing sites (i.e., Eberswalde, Gale, and Holden) are basins. Phyllosilicates may have accumulated in basins by fluvial transportation of clay material, implying that the clay material may not have formed in-situ and clay-bearing materials instead may have been transported and collected in these basins where they were later lithified (e.g. Milliken and Bish 2010). Further analysis through MSL experiments may help determine if the observed clays at Gale were formed in-situ or were transported from another location.

The single exception to the above generalization is the clay-bearing material within the Eberswalde ellipse; it has a much higher thermal inertia (875 to 1165 $J\,m^{-2}\,K^{-1}\,s^{-1/2}$) than observed at other landing sites. The higher thermal inertia indicates a further degree of lithification (as compared to the other sites) or localized alteration of bedrock. In this case, we argue that the clay-bearing material at Eberswalde is altered bedrock and may indicate localized alteration at this site, possibly from water ponding in the Eberswalde basin or in an aquifer.

8 Conclusions

The thermal inertia of all these sites is higher than those observed at either MER landing site from orbit (Golombek et al. 2003, 2005; Fergason et al. 2006b). Therefore MSL will likely land on a site with fundamentally different thermophysical properties than observed in situ previously. All sites contain morphologic, mineralogical, and thermophysical variability. This work has described the physical properties of the surface at these sites and determined how thermophysical variations correspond to morphology, and when applicable mineralogical diversity. The additional insight gained through the analysis of thermophysical data sets and the integration of thermal inertia with morphological and chemical information has enabled further exploration of the physical characteristics of the surface and why these characteristics vary.

Eberswalde

- At 100 m/pixel, the proportion of dark, likely unconsolidated or very slightly indurated material relative to exposed bedrock or highly indurated surfaces controls the thermal inertia of a given region. So generally speaking, lower thermal inertia surfaces have more unconsolidated material present, typically expressed as dark deposits that typically include bed forms. Higher thermal inertia surfaces consist of more exposed bedrock or the presence of more rocky material.
- Eberswalde is the only candidate site whose thermal inertia values are consistent with bedrock (thermal inertia values of 875 to 1165 $J\,m^{-2}\,K^{-1}\,s^{-1/2}$) exposed at the surface at scales larger than 100 m. Interestingly, this exposed bedrock is also clay-bearing.
- Clays within the delta to the west of the ellipse have a thermal inertia of 545 to 730 $J\,m^{-2}\,K^{-1}\,s^{-1/2}$, and this thermal inertia range is more consistent with other clay-bearing surfaces observed in the MSL candidate landing sites. The clay-bearing material is relatively bright, layered material with darker, likely unconsolidated material intermixed.

Gale

- The majority of the ellipse has a moderate thermal inertia (250 to 410 $J\,m^{-2}\,K^{-1}\,s^{-1/2}$), which is likely an indurated surface with unconsolidated materials present. The surface texture within this moderate material range is consistent throughout the majority of the ellipse and appears extensively degraded in visible images.
- The primary difference between higher and moderate thermal inertia surfaces may be due to the amount of mantling material present. This relationship suggests that the mantling material was likely formed in a similar way, and the post-emplacement modification of this material is the primary distinguishing factor.
- In the western portion of the ellipse, an ancient fan deposit originates in the mouth of a channel and encompasses approximately one-third of the ellipse. The fan is roughly half lower thermal inertia (275 to 380 $J\,m^{-2}\,K^{-1}\,s^{-1/2}$) and half higher thermal inertia (395 to 555 $J\,m^{-2}\,K^{-1}\,s^{-1/2}$). The southern portion of the fan has the largest single exposure of high thermal inertia material in the ellipse, and is therefore a region of high interest. Although this material is likely well indurated, the many sinuous ridges may be difficult to traverse.
- Outcrops of higher standing material are observed throughout the ellipse and suggest that this region was once covered by a layer of material that was more extensive in the past. One possible interpretation is that this surface is degraded, possibly caused by the removal of mound material that was once more extensive and potentially filling Gale crater.
- Individual layers in the mound are distinguishable in the thermal inertia data. Thus, the MSL rover could be traversing through materials that are compositionally diverse with distinct surface properties associated with individual units. The mound has been previously divided into a Lower and Upper formation (Milliken et al. 2010). In this work, the Lower formation was further divided into five thermophysical units that typically correspond to morphological and mineralogical boundaries. The entire lower mound has a thermal inertia ranging from 265 to 490 $J\,m^{-2}\,K^{-1}\,s^{-1/2}$.
- The Upper formation of the mound has a thermal inertia of 120 to 260 $J\,m^{-2}\,K^{-1}\,s^{-1/2}$, which suggests the presence of fine-grained, loosely consolidated material and a significant portion of dust covering the mound. However, thermophysical variations in the Upper formation correspond to specific layers and terraces observed in the mound. These variations may be caused by differing amounts of unconsolidated material and dust present, which may be controlled by topography.

Holden

- The mean thermal inertia within the Holden landing ellipse is 390 $J\,m^{-2}\,K^{-1}\,s^{-1/2}$ with a standard deviation of 25 $J\,m^{-2}\,K^{-1}\,s^{-1/2}$. As indicated by the low standard deviation, the majority of the ellipse has a consistent thermal inertia and there is little variation in surface properties. Holden has the least thermophysical diversity of the sites considered.
- The vast majority of the Holden ellipse has a thermal inertia of 340 to 475 $J\,m^{-2}\,K^{-1}\,s^{-1/2}$ and consists of bed forms with some consolidated material intermixed. The thermal inertia is higher than expected for bed forms on Mars and may indicate that the bed forms may be indurated, consist of a predominant grain size larger than sand, or that the thickness of the unconsolidated material is thin enough in places that the thermal inertia is influenced by underlying, well indurated material or bedrock.
- In the far southern portion of the ellipse and along a potential traverse route, brighter layered deposits and dark sand have a high thermal inertia (450 $J\,m^{-2}\,K^{-1}\,s^{-1/2}$ to 600 $J\,m^{-2}\,K^{-1}\,s^{-1/2}$). These deposits also contain clay-bearing minerals (Milliken and

Bish 2010). Due to the sub-pixel mixing of materials, and the small size of the bright layered outcrops relative to the THEMIS field-of-view, it is not possible to isolate the thermal inertia of this clay-rich material with confidence. The highest thermal inertia values observed are ~600 $J\,m^{-2}\,K^{-1}\,s^{-1/2}$, which suggests that the layers themselves are well-indurated sediment or weathered bedrock.

Mawrth Vallis

- Mawrth Vallis has the most thermophysical diversity of any of the proposed landing sites. Within the Mawrth Vallis landing ellipse, the mean thermal inertia is 310 $J\,m^{-2}\,K^{-1}\,s^{-1/2}$. A wide variety of materials contribute to the moderate thermal inertia surfaces, including a mixture of bedrock, indurated surfaces, bed forms, and unconsolidated fines. It is also possible that the degree of bedrock weathering varies throughout the region (e.g., Fergason et al. 2006b).
- There are two distinct clay signatures within the landing ellipse: Fe/Mg-smectite and Al-phyllosilicate, and these signatures have distinct thermophysical properties. The thermal inertia of the Fe/Mg smectite-bearing material ranges from 400 to 470 $J\,m^{-2}\,K^{-1}\,s^{-1/2}$, the highest thermal inertia value in the landing ellipse. The Fe/Mg-smectite clays are also the brightest material in the landing ellipse, form sinuous ridges, and contain fractures and polygons filled with dark, probably aeolian material. This dark, aeolian material is lowering the overall apparent thermal inertia value interpreted from THEMIS data, therefore, this clay material is likely very well indurated.
- The Al-phyllosilicate-bearing material has a variable thermal inertia ranging from 210 to 390 $J\,m^{-2}\,K^{-1}\,s^{-1/2}$. This material is also layered and rough, but has significantly more dark, aeolian material present on the surface. It is also not as bright as the Fe/Mg-smectite area. The variable thermal inertia and difference in brightness may both be related to this additional unconsolidated material present and variations in the degree of weathering. Therefore, it is impossible to obtain accurate information regarding the physical properties of the phyllosilicates from the data available.

Acknowledgements Attendance at the landing site workshops greatly enhanced our understanding of various components of each site. Specifically, discussions with Kenneth Edgett (MSSS), Justin Hagerty (USGS), Michael Kraft (ASU), and Ashwin Vasavada (JPL) on various aspects related to these sites greatly helped place our findings in a broader context. Kenneth Herkenhoff (USGS), Kenneth Tanaka (USGS), Kenneth Edgett (MSSS), and an anonymous reviewer provided comments that greatly improved the presentation of this work. Trent Hare (USGS) and Ryan Luk (then at ASU) helped produce products that have been released to the public (http://astrogeology.usgs.gov/MSL/; http://themis.asu.edu/landingsites). Ryan Luk was invaluable for helping develop mosaic scripts and generating early versions of the daytime IR, nighttime IR, and visible mosaics and the nighttime IR over daytime IR overlay images available online. Daytime IR, nighttime IR, qualitative (8-bit) thermal inertia, and visible image mosaic generation for the initial 36 proposed landing sites (as of June 2006) was funded by the Mars Odyssey Project Office. The thermal inertia analysis and generation and analysis of predicted temperature maps were funded by a JPL subcontract through the Critical Data Products program.

Appendix: Thermal Inertia Derivation

The Thermal Emission Imaging Spectrometer (THEMIS) infrared (IR) data have an improved spatial resolution (100 m/pixel) over previous datasets, such as Mars Global Surveyor Thermal Emission Spectrometer (TES) or Viking Infrared Thermal Mapper. The THEMIS data set enables the modeling of surface physical characteristics to determine particle size

information and identify surface exposures of bedrock, and allows these physical properties to be correlated to morphologic features. This data set can also facilitate an improved understanding of geologic processes that have influenced the Martian surface.

To derive thermal inertia from THEMIS data, we used the method of Fergason et al. (2006a). The brightness temperature of the surface is first determined by fitting a Planck curve to band 9 (centered at 12.57 μm) calibrated radiance that has been corrected for instrumental effects. This wavelength range was chosen because it has the highest signal to noise ratio and is relatively insensitive to atmospheric dust. The THEMIS band 9 temperatures are converted to a thermal inertia by interpolation within a 7-dimensional look-up table using latitude, season, local solar time, atmospheric dust opacity, thermal inertia, elevation (atmospheric pressure), and albedo as input parameters.

The look-up table includes a thermal inertia range of 24 to 3000 $\mathrm{J\,m^{-2}\,K^{-1}\,s^{-1/2}}$, and values exceeding 1800 have been observed (e.g. Edwards et al. 2009). This thermal inertia range is significantly larger than that used in the TES standard model (maximum of 800), and allows the detection of exposures of consolidated materials or bedrock on the surface. This extended thermal inertia range was required because of: (1) the higher spatial resolution of THEMIS; (2) initial results from THEMIS nighttime temperatures suggesting the presence of bedrock (e.g. Christensen et al. 2003); and (3) the fact that many regions on Mars were saturated at the maximum value of thermal inertia in the TES model (Fergason et al. 2006a).

This look-up table is generated using a thermal model developed by H. H. Kieffer, which was derived from the Viking IRTM thermal model (Kieffer et al. 1977) with several modifications, the most significant being an improved atmospheric component. This improved atmospheric component consists of a one-layer atmosphere that is spectrally gray at solar wavelengths with the direct and diffuse illuminations computed using a 2-stream delta-Eddington model. The effects of 3-dimensional blocks on the surface, condensate clouds, and the latent heat of water ice are not considered (Kieffer 2011). This model can incorporate the effects of a radiatively-coupled sloping surface at any azimuth, but for the nominal thermal inertia calculations, slopes are not considered. Generally, slopes below 10° at all azimuths have a small effect on the nighttime surface temperature, and therefore the thermal inertia. Higher slope angles may be problematic, but this conclusion is dependent on the slope azimuth and the season. Due to the potential for slopes to be a factor, surfaces with slopes greater than ∼10° were interpreted with caution (Fergason et al. 2006a).

Model parameters appropriate for the THEMIS image and the measured band 9 surface temperatures are then used to interpolate the thermal inertia between the calculated look-up table node values. Interpolation is performed on a pixel-by-pixel basis using season, latitude, and local solar time from spacecraft ephemeris. The remaining model input parameters are obtained from external datasets. The albedo of features in the THEMIS image is determined from the TES albedo binned at 8 pixels per degree (Christensen et al. 2001). Elevation information is ascertained from Mars Orbiter Laser Altimeter (MOLA) elevation (Zuber et al. 1992; Smith et al. 1999, 2001a) binned at 128 elements per degree. Finally, the opacity is inferred by using the THEMIS image season to select a TES dust opacity value from data binned at 0.3 pixel per degree in latitude and 0.13 pixel per degree in longitude for every 15° Ls during the first Martian year of MGS mapping (e.g. Smith et al. 2001b).

Uncertainties in the THEMIS derived thermal inertia values are primarily due to (1) instrument calibration; (2) uncertainties in model input parameters, including albedo and opacity, at the resolution of the THEMIS instrument; and (3) thermal model uncertainties. Random and systematic errors in the THEMIS surface measurements result in an absolute calibration accuracy of THEMIS nighttime temperature between 1.8 K and 2.8 K (Fergason et al. 2006a), and a relative precision of 1.2 K (P.R. Christensen, THEMIS calibration report, http://themis-data.asu.edu/pds/calib/calib.pdf, (2005) Accessed 15 August 2011). TES

albedo, TES atmospheric dust opacity, and MOLA elevation values are incorporated as model input parameters at a coarser resolution than that of the THEMIS temperature data, and thus may not be adequately taking into account the effects of these parameters on the thermal inertia derivation. TES atmospheric dust opacity is used for the first Martian year of MGS mapping when there were no global dust storms (Smith et al. 2000, 2001b). We assume that the amount of dust in the atmosphere is repeatable from year to year; this has been shown to be a reasonable approximation during seasons devoid of major dust storms (Clancy et al. 2000; Smith 2004). To avoid dusty atmospheric conditions, we do not determine thermal inertia when the atmospheric opacity is greater than 0.40 (visible wavelength). Elevation (used to determine the atmospheric pressure) has a minor effect on the thermal inertia, and the atmospheric dust opacity does not vary significantly over the area of a THEMIS image (Clancy et al. 2000; Smith et al. 2001b), so these two approximations are likely adequate. However, sub-TES-pixel variations in albedo that affect the nighttime surface temperature in THEMIS data likely affect the accuracy at which thermal inertia values can be calculated, and regions where albedo is varying over short distances (less than 3 km) are interpreted with caution. Considering the uncertainties in both the THEMIS instrument calibration and input parameters, the absolute accuracy of the THEMIS thermal inertia is ∼20 % (for additional detail, see Fergason et al. 2006a).

References

R.B. Anderson, J.F. Bell III, Geologic mapping and characterization of Gale Crater and implications for its potential as a Mars Science Laboratory landing site. Mars **5**, 76–128 (2010). doi:10.1555/mars.2010.0004

R.E. Arvidson et al., Overview of the spirit Mars exploration rover mission to Gusev Crater: landing site to backstay rock in the Columbia Hills. J. Geophys. Res. **111**, E02S01 (2006). doi:10.1029/2005JE002499

J.L. Bandfield, D. Rogers, M.D. Smith, P.R. Christensen, Atmospheric correction and surface spectral unit mapping using thermal emission imaging system data. J. Geophys. Res. **109**, E10008 (2004). doi:10.1029/2004JE002289

J.L. Bandfield, A.D. Rogers, C.S. Edwards, The role of aqueous alteration in the formation of martian soils. Icarus **211**, 157–171 (2011). doi:10.1016/j.icarus.2010.08.028

J.-P. Bibring et al., Global mineralogical and aqueous Mars history derived from OMEGA/Mars express data. Science **312**, 400–404 (2006). doi:10.1126/science.1122659

N.A. Cabrol, E.A. Grin, Distribution, classification, and ages of martian impact crater lakes. Icarus **142**, 160–172 (1999)

N.A. Cabrol, E.A. Grin, H.E. Newsom, R. Landheim, C.P. McKay, Hydrogeologic evolution of Gale Crater and its relevance to the exobiological exploration of Mars. Icarus **139**, 235–245 (1999)

P.R. Christensen, D.L. Anderson, S.C. Chase, R.N. Clark, H.H. Kieffer, M.C. Malin, J.C. Pearl, J. Carpenter, N. Bandiera, F.G. Brown, S. Silverman, Thermal emission spectrometer experiment: Mars observer mission. J. Geophys. Res. **97**(E5), 7719–7734 (1992)

P.R. Christensen, J.L. Bandfield, V.E. Hamilton, S.W. Ruff, H.H. Kieffer, T.N. Titus, M.C. Malin, R.V. Morris, M.D. Lane, R.L. Clark, B.M. Jakosky, M.T. Mellon, J.C. Pearl, B.J. Conrath, M.D. Smith, R.T. Clancy, R.O. Kuzmin, T. Roush, G.L. Mehall, N. Gorelick, K. Bender, K. Murray, S. Dason, E. Greene, S. Silverman, M. Greenfield, Mars global surveyor thermal emission spectrometer experiment: investigation description and surface science results. J. Geophys. Res. **106**(E10), 23,823–23,871 (2001)

P.R. Christensen, J.L. Bandfield, J.F. Bell III, N. Gorelick, V.E. Hamilton, A. Ivanov, B.M. Jakosky, H.H. Kieffer, M.D. Lane, M.C. Malin, T. McConnochie, A.S. McEwen, H.Y. McSween Jr., G.L. Mehall, J.E. Moersch, K.H. Nealson, J.W. Rice Jr., M.I. Richardson, S.W. Ruff, M.D. Smith, T.N. Titus, M.B. Wyatt, Morphology and composition of the surface of Mars: Mars Odyssey THEMIS results. Science **300**(5628), 2056–2061 (2003)

P.R. Christensen, B.M. Jakosky, H.H. Kieffer, M.C. Malin, H.Y. McSween Jr., K. Nealson, G.L. Mehall, S.H. Silverman, S. Ferry, M. Caplinger, M. Ravine, The Thermal Emission Imaging System (THEMIS) for the Mars 2001 Odyssey mission. Space Sci. Rev. **110**, 85–130 (2004)

R.T. Clancy, B.J. Sandor, M.J. Wolff, P.R. Christensen, M.D. Smith, J.C. Pearl, B.J. Conrath, R.J. Wilson, An intercomparison of ground-based millimeter, MGS TES, and Viking atmospheric temperature measurements: seasonal and interannual variability of temperatures and dust loading in the global Mars atmosphere. J. Geophys. Res. **105**(E4), 9553–9571 (2000)

K.S. Edgett, P.R. Christensen, The particle size of Martian aeolian dunes. J. Geophys. Res. **96**(E5), 22,765–22,776 (1991)
C.S. Edwards, J.L. Bandfield, P.R. Christensen, R.L. Fergason, Global distribution of bedrock exposures on Mars using THEMIS high-resolution thermal inertia. J. Geophys. Res. **114**, E11001 (2009). doi:10.1029/2009JE003363
R.L. Fergason, P.R. Christensen, Formation and erosion of layered materials: geologic and dust cycle history of eastern Arabia Terra, Mars. J. Geophys. Res. **113**, E12001 (2008). doi:10.1029/2007JE002973
R.L. Fergason, P.R. Christensen, H.H. Kieffer, High-resolution thermal inertia derived from the Thermal Emission Imaging System (THEMIS): thermal model and applications. J. Geophys. Res. **111**, E12004 (2006a). doi:10.1029/2006JE002735
R.L. Fergason, P.R. Christensen, J.F. Bell III, M.P. Golombek, K.E. Herkenhoff, H.H. Kieffer, Physical properties of the Mars exploration rover landing sites as inferred from Mini-TES derived thermal inertia. J. Geophys. Res. **111**(E2), E02S21 (2006b). doi:10.1029/2005JE002583
J.A. Fountain, E.A. West, Thermal conductivity of particulate basalt as a function of density in simulated lunar and martian environments. J. Geophys. Res. **75**(20), 4063–4069 (1970)
M.P. Golombek, J.A. Grant, T.J. Parker, D.M. Bass, J.A. Crisp, S.W. Squyres, A.F.C. Haldemann, M. Adler, W.J. Lee, N.T. Bridges, R.E. Arvidson, M.H. Carr, R.L. Kirk, P.C. Knocke, R.B. Roncoli, C.M. Weitz, J.T. Schofield, R.W. Zurek, P.R. Christensen, R.L. Fergason, F.S. Anderson, J.W. Rice, Selection of the Mars exploration rover landing sites. J. Geophys. Res. **108**, 8072 (2003). doi:10.1029/2003JE002074
M.P. Golombek, R.E. Arvidson, J.F. Bell III, P.R. Christensen, J.A. Crisp, L.S. Crumpler, B.L. Ehlmann, R.L. Fergason, J.A. Grant, R. Greeley, A.F.C. Haldemann, D.M. Kass, T.J. Parker, J.T. Schofield, S.W. Squyres, R.W. Zurek, Assessment of Mars exploration rover landing site predictions. Nature **436**, 44–48 (2005). doi:10.1038/nature03600
M.P. Golombek et al., Selection of the Mars science laboratory landing site. Space Sci. Rev., this issue (2012)
J.L. Gooding, Chemical weathering on Mars: thermodynamic stabilities of primary minerals (and their alteration products) from mafic igneous rocks. Icarus **33**, 485–513 (1978)
J.A. Grant, T.J. Parker, Drainage evolution in the Margaritifer Sinus region, Mars. J. Geophys. Res. **107**, 5066 (2002). doi:10.1029/2001JE001678
J.A. Grant, R.P. Irwin III, J.P. Grotzinger, R.E. Milliken, L.L. Tornabene, A.S. McEwen, C.M. Weitz, S.W. Squyres, T.D. Glotch, B.J. Thomson, HiRISE imaging of impact megabreccia and sub-meter aqueous strata in Holden Crater, Mars. Geology **36**, 195–198 (2008). doi:10.1130/G24340A.1
J.A. Grant et al., The science process for selecting the landing site for the 2011 Mars Science Laboratory. Planet. Space Sci. **59**, 1114–1127 (2011). doi:10.1016/j.pss.2010.06.016
R. Greeley, J.E. Guest, Geologic map of the eastern equatorial region of Mars, U.S. Geol. Surv. Misc. Invest. Map, I-1802-B (1987)
J. Grotzinger et al., Mars science laboratory mission, science investigation. Space Sci. Rev. (2012). doi:10.1007/s11214-012-9892-2
S.W. Hobbs, D.J. Paull, M.C. Bourke, Aeolian processes and dune morphology in Gale Crater. Icarus **210**, 102–115 (2010). doi:10.1016/j.icarus2010/06/006
B.M. Jakosky, The effects of nonideal surfaces on the derived thermal properties of Mars. J. Geophys. Res. **84**(B14), 8252–8262 (1979)
D.J. Jerolmack, D. Mohrig, M.T. Zuber, S. Byrne, A minimum time for the formation of Holden Northeast fan, Mars. Geophys. Res. Lett. **31**, L21701 (2004). doi:10.1029/2004GL021326
H.H. Kieffer, personal communciation (2011)
H.H. Kieffer, S.C. Chase Jr., E. Miner, G. Münch, G. Neugebauer, Preliminary report on infrared radiometric measurements from the Mariner 9 spacecraft. J. Geophys. Res. **78**(20), 4291–4312 (1973)
H.H. Kieffer, T.Z. Martin, A.R. Peterfreund, B.M. Jakosky, E.D. Miner, F.D. Palluconi, Thermal and albedo mapping of Mars during the Viking primary mission. J. Geophys. Res. **82**(28), 4249–4291 (1977)
K.W. Lewis, O. Aharonson, Stratigraphic analysis of the distributary fan in Eberswalde crater using stereo imagery. J. Geophys. Res. **111**, E06001 (2006). doi:10.1029/2005JE002558
K. Lewis, O. Aharonson, J. Grotzinger, R. Kirk, A. McEwen, T. Suer, Quasi periodic bedding in the sedimentary rock record of Mars. Science **322**, 1532–1535 (2008). doi:10.1126/science.1161870
M.C. Malin, K.S. Edgett, Sedimentary rocks of early Mars. Science **290**, 1927–1937 (2000)
M.C. Malin, K.S. Edgett, Mars global surveyor Mars orbiter camera: interplanetary cruise through primary mission. J. Geophys. Res. **106**, 23429–23570 (2001). doi:10.1029/2006JE002808
M.C. Malin, K.S. Edgett, Evidence for persistent flow and aqueous sedimentation on early Mars. Science **302**, 1931–1934 (2003)
M.C. Malin, G.E. Danielson, A.P. Ingersoll, H. Masursky, J. Veverka, M.A. Ravine, T.A. Soulanille, Mars observer camera, J. Geophys. Res. **97**(E5), 7699–7718 (1992)

M.C. Malin, J.F. Bell III, B.A. Cantor, M.A. Caplinger, W.M. Calvin, R.T. Clancy, K.S. Edgett, L. Edwards, R.M. Haberle, P.B. James, S.W. Lee, M.A. Ravine, P.C. Thomas, M.J. Wolff, Context camera investigation on board the Mars reconnaissance orbiter. J. Geophys. Res. **112**, E05S04 (2007). doi:10.1029/2006JE002808

A.S. McEwen et al., Mars reconnaissance orbiter's high resolution imaging science experiment (HiRISE). J. Geophys. Res. **112**, E05S02 (2007). doi:10.1029/2005JE002605

M.T. Mellon, B.M. Jakosky, H.H. Kieffer, P.R. Christensen, High-resolution thermal inertia mapping from the Mars global surveyor thermal emission spectrometer. Icarus **148**, 437–455 (2000)

J.R. Michalski, E.Z. Noe Dobrea, Evidence for a sedimentary origin of clay minerals in the Mawrth Vallis region, Mars. Geology **35**, 951–954 (2007). doi:10.1130/G23854A.1

J.R. Michalski, R.L. Fergason, Composition and thermal inertia of the Mawrth Vallis region of Mars from TES and THEMIS data. Icarus **199**, 25–48 (2009)

J.R. Michalski, J.-P. Bibring, F. Poulet, D. Loizeau, N. Mangold, E. Noe Dobrea, J.L. Bishop, J.J. Wray, N.K. McKeown, M. Parente, E. Hauber, F. Altieri, F.G. Carrozzo, P.B. Niles, The Mawrth Vallis region of Mars: a potential landing site for the Mars science laboratory (MSL) mission. Astrobiology **10**(7), 687–703 (2010). doi:10.1089/ast.2010.0491

R.E. Milliken, D.L. Bish, Sources and sinks of clay minerals on Mars. Philos. Mag. **90**, 2293–2308 (2010). doi:10.1080/14786430903573132

R.E. Milliken, J.P. Grotzinger, B.J. Thomson, Paleoclimate of Mars as captured by the stratigraphic record in Gale Crater. Geophys. Res. Lett. **37**, L04201 (2010). doi:10.1029/2009GL041870

J.M. Moore, A.D. Howard, Large alluvial fans on Mars. J. Geophys. Res. **110**, E04005 (2005). doi:10.1029/2004JE002352

G. Neugebauer, G. Münch, H. Kieffer, S.C. Chase Jr., E. Miner, Mariner 1969 infrared radiometer results: temperature sand thermal properties of the martian surface. Astron. J. **76**(8), 719–728 (1971)

F.D. Palluconi, H.H. Kieffer, Thermal inertia mapping of Mars from 60° S to 60° N. Icarus **45**, 415–426 (1981)

S.M. Pelkey, B.M. Jakosky, Surficial geologic surveys of Gale Crater and Melas Chasma, Mars: integration of remote-sensing data. Icarus **160**, 228–257 (2002)

S.M. Pelkey, B.M. Jakosky, P.R. Christensen, Surficial properties in Gale Crater, Mars, from Mars Odyssey THEMIS data. Icarus **167**, 244–270 (2004)

J.B. Pollack, M.E. Ockert-Bell, M.E. Shepard, Viking Lander image analysis of martian atmospheric dust. J. Geophys. Res. **100**(E3), 5235–5250 (1995)

M. Pondrelli, A. Baliva, S. Di Lorenzo, L. Marinangeli, A.P. Rossi, Complex evolution of paleolacustrine systems on Mars: an example from the Holden crater. J. Geophys. Res. **110**, E04016 (2005). doi:10.1029/2004JE002335

M. Pondrelli, A.P. Rossi, L. Marinangeli, E. Huger, K. Gwinner, A. Baliva, S. Di Lorenzo, Evolution and depositional environments of the Eberswalde fan delta, Mars. Icarus **197**, 429–451 (2008). doi:10.1016/j.icarus.2008.05.018

F. Poulet, J.-P. Bibring, J.F. Mustard, A. Gendrin, N. Mangold, Y. Langevin, R.E. Arvidson, B. Gondet, C. Gomez, OMEGA Team, Phyllosilicates on Mars and implications for early martian climate. Nature **438**, 623–627 (2005)

F. Poulet, N. Mangold, D. Loizeau, J.-P. Bibring, Y. Langevin, J. Michalski, B. Gondet, Abundance of minerals in the phyllosilicate-rich units on Mars. Astron. Astrophys. **487**, L41–L44 (2008)

M.A. Presley, P.R. Christensen, Thermal conductivity measurements of particulate materials, 2: results. J. Geophys. Res. **102**, 6551–6566 (1997)

N.E. Putzig, M.T. Mellon, Thermal behavior of horizontally mixed surfaces on Mars. Icarus **191**, 52–67 (2007a). doi:10.1016/j.icarus.2007.03.022

N.E. Putzig, M.T. Mellon, Apparent thermal inertia and the surface heterogeneity of Mars. Icarus **191**, 68–94 (2007b). doi:10.1016/j.icarus.2007.05.013

M.S. Rice, S. Gupta, J.F. Bell III, N.H. Warner, Influence of fault-controlled topography on fluviodeltaic sedimentary systems in Eberswalde crater, Mars. Geophys. Res. Lett. **38**, L16203 (2011). doi:10.1029/2011GL048149

A.P. Rossi, G. Neukum, M. Pondrelli, S. van Gasselt, T. Zegers, E. Hauber, A. Chicarro, B. Foing, Large-scale spring deposits on Mars? J. Geophys. Res. **113**, E08016 (2008). doi:10.1029/2007JE003062

S.W. Ruff, P.R. Christensen, Bright and dark regions on Mars: particle size and mineralogical characteristics based on Thermal Emission Spectrometer data. J. Geophys. Res. **107**, E12 (2002). doi:10.1029/2001JE001580

P.H. Schultz, A.B. Lutz, Polar wandering of Mars. Icarus **73**, 91–141 (1988)

D.H. Scott, K.L. Tanaka, Geologic map of the western equatorial region of Mars, US Geological Survey Miscellaneous Investigation Series, Map I-1802-A, scale 1:15,000,000 (1986)

D.H. Scott, M.G. Chapman, Geologic and topographic maps of the Elysium paleolake basin, Mars, United States Geological Survey Series, Map I-2397, scale 1:5,000,000 (1995)
M.D. Smith, Interannual variability in TES atmospheric observations of Mars during 1999–2003. Icarus **167**, 148–165 (2004)
D. Smith, M. Zuber, S. Solomon, R. Phillips, J. Head, J. Garvin, W. Banerdt, D. Muhlemann, G. Pettengill, G. Neumann, F. Lemoine, J. Abshire, O. Aharonson, C. Brown, S. Hauck, A. Ivanov, P. McGovern, H. Zwally, T. Duxbury, The global topography of Mars and implications for surface evolution. Science **284**, 1495–1503 (1999)
M.D. Smith, J.C. Pearl, B.J. Conrath, P.R. Christensen, Mars global surveyor thermal emission spectrometer (TES) observations of dust opacity during aerobreaking and science phasing. J. Geophys. Res. **105**(E4), 9539–9552 (2000)
D.E. Smith, M.T. Zuber, H.V. Frey, J.B. Garvin, J.W. Head, D.O. Muhleman, G.H. Pettengill, R.J. Phillips, S.C. Solomon, H.J. Zwally, W.B. Banerdt, T.C. Duxbury, M.P. Golombek, F.G. Lemoine, G.A. Neumann, D.D. Rowlands, O. Aharonson, P.G. Ford, A.B. Ivanov, C.L. Johnson, P.J. McGovern, J.B. Abshire, R.S. Afzal, X. Sun, Mars orbiter laser altimeter: experiment summary after the first year of global mapping of Mars. J. Geophys. Res. **106**(E10), 23,689–23,722 (2001a)
M.D. Smith, J.C. Pearl, B.J. Conrath, P.R. Christensen, One martian year of atmospheric observations by the thermal emission spectrometer. Geophys. Res. Lett. **28**(22), 4263–4266 (2001b)
S.W. Squyres et al., The Spirit Rover's Athena science investigation at Gusev Crater, Mars. Science **305**, 794–799 (2004)
R. Sullivan, R. Arvidson, J.F. Bell III, R. Gellert, M. Golombek, R. Greeley, K. Herkenhoff, J. Johnson, S. Thompson, P. Whelley, J. Wray, Wind-driven particle mobility on Mars: insights from Mars exploration rover observations at "El Dorado" and surroundings at Gusev Crater. J. Geophys. Res. **113**, E06S07 (2008). doi:10.1029/2008JE003101
R.E. Summons, J.P. Amend, D. Bish, R. Buick, G.D. Cody, D.J. Des Marais, G. Dromart, J.L. Eigenbrode, A.H. Knoll, D.Y. Sumner, Preservation of martian organic and environmental records: final report of the Mars biosignature working group. Astrobiology **11**(2), 157–181 (2011). doi:10.1089/a/st.2010.0506
B.J. Thomson, N.T. Bridges, R. Milliken, A. Baldridge, S.J. Hook, J.K. Crowley, G.M. Marion, C.R. de Souza Filho, A.J. Brown, C.M. Weitz, Constraints on the origin and evolution of the layered mound in Gale Crater, Mars using Mars reconnaissance orbiter data. Icarus **214**, 413–432 (2011). doi:10.1016/j.icarus.2011.02.002
M.G. Tomasko, L.R. Doose, M. Lemmon, P.H. Smith, E. Wegryn, Properties of dust in the martian atmosphere from the imager on Mars pathfinder. J. Geophys. Res. **104**, 8987–9007 (1999)
A.F. Vaughan et al., Pancam and microscopic imager observations of dust on the Spirit rover: cleaning events, spectral properties, and aggregates. Mars **5**, 129–145 (2010). doi:10.1555/mars.2010.0005
A.E. Wechsler, P.E. Glaser, Pressure effects on postulated lunar materials. Icarus **4**, 352–377 (1965)
C.K. Wentworth, A scale of grade and class terms for clastic sediments. J. Geol. **30**, 377–392 (1922)
S.A. Wilson, A.D. Howard, J.A. Grant, Geomorphic and stratigraphic analysis of Crater Terby and layered deposits north of Hellas basin, Mars. J. Geophys. Res. **112**, E08009 (2007). doi:10.1029/2006JE002830
M.J. Wolff, R.T. Clancy, Constraints on the size of martian aerosols from thermal emission spectrometer observations. J. Geophys. Res. **108**, E9 (2003). doi:10.1029/2003JE002057
M.J. Wolff et al., Constraints on dust aerosols from the Mars exploration rovers using MGS overflights and Mini-TES. J. Geophys. Res. **111**, E12S17 (2006). doi:10.1029/2006JE002786
W. Woodside, J.H. Messmer, Thermal conductivity of porous media, I: unconsolidated sands. J. Appl. Phys. **32**(9), 1688–1699 (1961)
J.J. Wray, B.L. Ehlmann, S.W. Squyres, J.F. Mustard, R.L. Kirk, Compositional stratigraphy of clay-bearing layered deposits at Mawrth Vallis, Mars. Geophys. Res. Lett. **35**, L12202 (2008). doi:10.1029/2008GL034385
M.T. Zuber, D.E. Smith, S.C. Solomon, D.O. Muhleman, J.W. Head, J.B. Garvin, J.B. Abshire, J.L. Bufton, The Mars observer laser altimeter investigation. J. Geophys. Res. **97**(E5), 7781–7797 (1992)